

Ion elemental-optimized layered double hydroxide nanoparticles promote chondrogenic differentiation and intervertebral disc regeneration of mesenchymal stem cells through focal adhesion signaling pathway

Zhaojie Wang^{a,b,1}, Huiyi Yang^{a,b,1}, Xu Xu^{a,b,1}, Hongxing Hu^{a,b}, Yuxin Bai^{a,b}, Jian Hai^{a,b}, Liming Cheng^{a,b,**}, Rongrong Zhu^{a,b,*}

^a Key Laboratory of Spine and Spinal Cord Injury Repair and Regeneration of Ministry of Education, Department of Orthopedics, Tongji Hospital Affiliated to Tongji University, School of Life Science and Technology, Tongji University, Shanghai, 200065, China

^b Frontier Science Center for Stem Cell Research, Tongji University, Shanghai, 200065, China

ARTICLE INFO

Keywords:

Mesenchymal stem cells
Layered double hydroxide
Chondrogenic differentiation
Intervertebral disc degeneration
Focal adhesion signaling pathway

ABSTRACT

Chronic low back pain and dyskinesia caused by intervertebral disc degeneration (IDD) are seriously aggravated and become more prevalent with age. Current clinical treatments do not restore the biological structure and inherent function of the disc. The emergence of tissue engineering and regenerative medicine has provided new insights into the treatment of IDD. We synthesized biocompatible layered double hydroxide (LDH) nanoparticles and optimized their ion elemental compositions to promote chondrogenic differentiation of human umbilical cord mesenchymal stem cells (hUC-MSCs). The chondrogenic differentiation of LDH-treated MSCs was validated using Alcian blue staining, qPCR, and immunofluorescence analyses. LDH-pretreated hUC-MSCs were differentiated prior to transplantation into the degenerative site of a needle puncture IDD rat model. Repair and regeneration evaluated using X-ray, magnetic resonance imaging, and tissue immunostaining 4–12 weeks after transplantation showed recovery of the disc space height and integrated tissue structure. Transcriptome sequencing revealed significant regulatory roles of the extracellular matrix (ECM) and integrin receptors of focal adhesion signaling pathway in enhancing chondrogenic differentiation and thus prompting tissue regeneration. The construction of ion-specific LDH nanomaterials for *in situ* intervertebral disc regeneration through the focal adhesion signaling pathway provides theoretical basis for clinical transformation in IDD treatment.

1. Introduction

The intervertebral disc (IVD) is the fibrous cartilage structure connecting adjacent vertebral bodies in the spine. IVD mainly contains the elastic and gelatinous constitute of nucleus pulposus (NP) in the central part, and the surrounding annulus fibrosus (AF) to support the NP function and provide nutrition [1,2]. The entire function of IVD has the function of buffering shock, protecting spinal cord and maintaining the motor function between vertebral bodies [3,4]. With increasing age, the proportion of components in the IVD become unbalanced, such as

decreased water content and collagen contents. The resulting decrease in disc elasticity eventually leads to the occurrence of IVD degeneration (IDD) [5]. Clinically, low back pain and symptoms of nerve root compression caused by IDD seriously affects the quality of life in patients, which affected 80% people at least once in their life [6,7]. Current IDD therapeutic strategies include artificial IVD replacement and transplantation of autologous and allogeneic materials transplantation, while neither of these strategies could reverse the pathological state of IDD [8–10].

The interaction mechanism of IDD is complicated and caused by

Peer review under responsibility of KeAi Communications Co., Ltd.

* Corresponding author. Key Laboratory of Spine and Spinal Cord Injury Repair and Regeneration of Ministry of Education, Department of Orthopedics, Tongji Hospital Affiliated to Tongji University, School of Life Science and Technology, Tongji University, Shanghai, 200065, China.

** Corresponding author. Key Laboratory of Spine and Spinal Cord Injury Repair and Regeneration of Ministry of Education, Department of Orthopedics, Tongji Hospital Affiliated to Tongji University, School of Life Science and Technology, Tongji University, Shanghai, 200065, China.

E-mail addresses: limingcheng@tongji.edu.cn (L. Cheng), rrzhu@tongji.edu.cn (R. Zhu).

¹ These authors contributed equally to this work.

<https://doi.org/10.1016/j.bioactmat.2022.08.023>

Received 17 May 2022; Received in revised form 1 August 2022; Accepted 22 August 2022

2452-199X/© 2022 The Authors. Publishing services by Elsevier B.V. on behalf of KeAi Communications Co. Ltd. This is an open access article under the CC BY-NC-ND license (<http://creativecommons.org/licenses/by-nc-nd/4.0/>).

many factors [11], mainly including the reduction of collagen and tissue extracellular matrix (ECM) components, which effectively resist external compression and maintain the ability of AF and NP tissues [12, 13]. When the ECM is affected during the IDD process, the function of NP is extensively disrupted owing to reduced water storage, retention capacity, and nutrient transportation. These reductions accelerate the devastating effects of degeneration [14,15]. Effective enrichment of collagen and ECM has been recognized as a potential strategy for the treatment of IDD [16]. Therefore, transplantation of stem cells that proliferate, self-renew, and differentiate has become a research focus [17,18]. Mesenchymal stem cells (MSCs) can be acquired from many sources and are thus considered a potential biological means of IDD therapy. Relevant attributes of MSCs include their self-renewal ability, potential for chondrogenic differentiation and production of ECM to refill the disc and restore the damaged tissue, and secretion of growth factors that regulate the inflammatory response and enhance tissue regeneration [19,20]. Commonly used MSCs include bone marrow MSCs (BMSCs), adipose stem cells (ASCs) and umbilical cord MSCs (UC-MSCs). Of these, UC-MSCs are more primitive and have a more pronounced ability to proliferate and differentiate [21–24]. Evidence showed that UC-MSCs could differentiate into cartilage faster than other MSCs. Compared with MSCs from other sources, MSCs derived from umbilical cords have the characteristics of easy collection, low immunogenicity, rapid self-renewal, stable multiplication rate and high proliferation capacity. Therefore, UC-MSCs are suitable for clinical research and application, and are preferred for cell therapy and regenerative medicine [25].

With the advanced use of MSCs in stem cell-mediated transplantation, effective functional optimization can improve the application outcomes [26–29]. Regulation of the fate of MSCs by bioactive materials could enable new theoretical strategies. Layered double hydroxide (LDH) is an anion-exchange nano clay with excellent biocompatibility, low cytotoxicity, anti-inflammatory, and degradation properties [30,31]. The physicochemical characteristics of LDH facilitate the binding of genes, drugs, and other biomaterials, which have been widely used in biomedical and tissue regenerative research [32–34]. Most studies have focused on the nanocarrier function of LDH. Our latest studies have shown that LDH can regulate the pluripotency and differentiation fate of stem cells, implicating LDH as an excellent tool for tissue regeneration and microenvironment regulation in regenerative therapy [35,36]. As the biological functions of LDH nanoparticles may differ under specific elemental compositions, further knowledge of the effect of optimized LDH on cell fate regulation of MSCs and IVD regeneration outcomes is needed.

In this study, LDH nanoparticles with different ions were synthesized, and co-cultured with human UC-MSCs (hUC-MSCs) to determine the optimal components of LDH that maximize the efficiency in promoting chondrogenic differentiation. Notably, the *in vivo* repair and regeneration efficacy of selected LDH pretreated hUC-MSCs in a rat IDD model was evaluated after *in situ* transplantation. Transcriptome analysis and subsequent experimental investigations were performed to elucidate the molecular mechanism of LDH-mediated promotion of the chondrogenesis of MSCs and facilitated tissue regeneration. By exploring the specific mechanisms of relevant intervention pathways in the regeneration and repair processes, the enhanced differentiation potential of treated MSCs can be fully utilized, thus providing new ideas and a scientific basis for the treatment of patients with IDD.

2. Materials and methods

2.1. LDH synthesis and characterization

Chemicals used for synthesizing LDH nanoparticles with elemental composition changes, including sodium hydroxide, magnesium chloride, aluminum chloride, ferric chloride, magnesium nitrate, aluminum nitrate and ferric nitrate were purchased from Sinopharm Chemical

Reagent Co., Ltd (Shanghai, China). The LDH nanoparticles were synthesized based on previously reported hydrothermal and coprecipitation methods [36]. For the different composition of MgAl–Cl, MgFe–Cl, MgAl–NO₃ and MgFe–NO₃ LDH, the initial respective reagents used were listed as follows: 0.6099 g magnesium chloride and 0.2414 g aluminum chloride (MgAl–Cl LDH), 0.6099 g magnesium chloride and 0.2703 g ferric chloride (MgFe–Cl LDH), 0.7692 g magnesium nitrate and 0.3751 g aluminum nitrate (MgAl–NO₃ LDH), and 0.7692 g magnesium nitrate and 0.303 g ferric nitrate (MgFe–NO₃ LDH).

The following procedures were the same for the four types of LDH nanoparticles. Briefly, 0.272 g sodium hydroxide was added to a three-necked round-bottomed flask and dissolved in 40 mL boiled distilled deionized water (ddH₂O) under an N₂ atmosphere to avoid the interference of CO₂. Each group of mixed powders was dissolved in 10 mL ddH₂O. After complete dissolution, the solution was poured into different three-necked flasks and stirred at 1000 rpm for 20 min. After stirring, the suspension was centrifuged at 8500 rpm for 10 min. The supernatant was discarded and the material was washed twice with ddH₂O. The final product was dissolved in 40 mL ddH₂O and placed in a hydrothermal kettle for a 16-h hydrothermal reaction at 100 °C. The obtained solution was centrifuged at 12,000 rpm for 15 min to collect the sediment and then washed three times with ddH₂O. Finally, the obtained four colloidal LDH was stored at 4 °C.

For the characterization of LDH materials, the samples were dropped onto a copper grid, the size and morphology of the particles were observed using a JEOL 1230 transmission electron microscope (TEM) with an accelerating voltage of 200 kV. For X-ray diffraction (XRD) analysis, LDH nanoparticles were freeze-dried and ground into homogeneous powder, the diffraction pattern of the sample was analyzed by Miniflex X-ray diffractometer from Rigaku (Japan). X-ray photoelectron spectroscopy (XPS) (ESCALAB 250XI, Thermo Fisher) was performed to analyze the elemental content of the samples. For Fourier transform infrared spectroscopy (FTIR) analysis, the samples were pressed with potassium bromide (KBr) into flakes, and the stretching vibration peaks of different groups were detected by molecular devices FTIR. The surface zeta potential of LDH was measured with Malvern nano Zetasizer. The material was dissolved in ddH₂O with a concentration of 0.5 mg/mL and ultrasonically dispersed.

2.2. Culture of hUC-MSCs

The hUC-MSCs were purchased from Cyagen Co. Ltd. (Guangzhou, China). The number of passages of cells used for the *in vitro* and *in vivo* experiments was controlled to within eight. Proliferation and differentiation medium were used. The proliferation culture medium was Dulbecco's modified Eagle's medium (DMEM)/F12 medium supplemented with 5% fetal bovine serum (Gibco, Franklin Lakes, NJ, USA) and 1% P/S (Gibco). The medium used for hUC-MSC chondrogenic differentiation was purchased from Cyagen, with DMEM high-glucose supplemented with dexamethasone (100 nM), ascorbic acid (50 mg/mL), and sodium pyruvate (100 mg/mL). And 10 ng/mL TGF-β3 was added in fresh cell culture medium ready to use.

2.3. Phenotypic identification of hUC-MSCs

The phenotypic identification kit of hUC-MSCs was purchased from Cyagen. Cells were seeded in a 6-well plate at a density of 2×10^5 cells/mL and cultured in the proliferation medium for 24 h. The cells were digested with trypsin, collected, incubated with primary antibodies to CD29, CD73, CD44, CD166, CD105, CD11b, CD34, and CD45 under dark conditions, and incubated at 4 °C for 30 min. After centrifugation at 3000 rpm for 5 min, the cells were washed twice and the corresponding secondary antibodies were added and incubated at 4 °C in the dark for 30 min. Goat anti FITC secondary antibody was used to label CD29, CD44, CD73, CD105, and CD166. Goat anti PE secondary antibody was used to label CD11b, CD14, CD34, and CD45. The sample was

centrifuged for the last time, resuspended in 500 μL of flow cytometry buffer, and then immediately examined using a model LSRFortessa flow cytometer (BD, Santa Clara, CA, USA).

2.4. Alcian blue staining

hUC-MSCs were seeded in a 24-well plate at 2×10^5 cells/mL with chondrogenic differentiation medium (Cyagen). When the cell density reached 80% after approximately 2 days, the cells were cultured with different LDH nanoparticles for 10 and 14 days of stimulation, and the medium was changed to maintain the differentiation environment. Samples were fixed with 4% paraformaldehyde (PFA) for 30 min and then treated with Alcian blue dye solution (KeyGEN BioTECH, Nanjing, China) for 30 min. The samples were examined using an optical microscope (Olympus, Tokyo, Japan). Stained sections were observed for chondrogenic differentiation and photographed according to cell morphology and staining depth.

2.5. Immunofluorescence staining

hUC-MSCs were cultured with different LDH (MgAl-Cl or MgFe-NO₃) for 14 days. Then, the cells in each group were fixed with 4% PFA (Sigma-Aldrich, St. Louis, MO, USA), permeabilized with 0.25% Triton X-100 (Amresco, Cleveland, OH, USA), blocked with 5% donkey serum (Jackson ImmunoResearch, West Grove, PA, USA), and primary SOX9 antibody (Abcam, Cambridge, MA, USA) was incubated at 4 °C overnight. The next day, the samples were conjugated with a fluorescent secondary antibody (Invitrogen, Carlsbad, CA, USA) at room temperature and nuclei were stained with 4',6-diamidino-2-phenylindole (DAPI; Abcam). The expression of key genes during chondrogenic differentiation was observed and photographed using a confocal microscope (Carl Zeiss). The excitation wavelength of DAPI was 405 nm and that of SOX9 was 488 nm.

For the pathway inhibition study, hUC-MSCs were cultured with MgFe-NO₃ LDH, Ac-PHSCN-NH₂ (ATN; Selleck, TX, USA), and LDH + ATN for 7 days. Immunofluorescence staining was performed after 7 days of culture. The staining steps were the same as above, and the primary antibody to integrin, was purchased from Abcam. Fluorescence was observed using a confocal microscope (Carl Zeiss). The excitation wavelengths were 405 nm for DAPI, 488 nm for SOX9, 647 nm for integrin, and 594 nm for F-actin.

2.6. Total mRNA extraction, cDNA reverse transcription and qPCR analysis

To detect the expression of chondrogenic genes and cell migration related genes, three repeated experiments were repeatedly performed for each group and qPCR. Total mRNA (500 ng) was extracted from hUC-MSCs using Trizol (Takara Bio, Shiga, Japan), and cDNA was reverse transcribed using the PrimeScript RT Kit (Takara Bio), followed by qPCR of 10 μL reaction volume (5 μL TB Green, 0.2 μL primer, 0.2 μL Rox reference dye, 1 μL cDNA, 3.6 μL H₂O) using TB Green Premix Ex Taq (Takara Bio, Japan). The qPCR primers are listed in [Supplementary Table S1](#).

2.7. Cell proliferation evaluation and by cell viability detection

For cell proliferation evaluation, hUC-MSCs were cultured with either MgAl-Cl or MgFe-NO₃ LDH for 24 h and 48 h. The cells were then incubated with EdU (Beyotime, Shanghai, China) for 2 h in the dark. The other steps were the same as those used for immunofluorescence staining. The excitation wavelength of EdU was 594 nm.

For cell viability analysis, hUC-MSCs were cultured with different LDH (MgAl-Cl or MgFe-NO₃) for 24 h and 72 h. The LDH solutions were prepared in fresh culture medium at concentrations of 1.0, 2.5, 5, 10, 20, and 50 $\mu\text{g}/\text{mL}$. Phosphate-buffered saline (PBS) was added to the blank

control group. Five replicates were performed for each group. 20 μL cell counting kit 8 (CCK8) solution was added to the orifice plate and incubated for 2 h in the dark. The optical density (OD) at 450 nm was detected using an enzyme-labeling instrument. The viability rate of the hUC-MSCs was calculated as follows:

$$\text{Cell viability \%} = \frac{\text{OD (Experimental group)}}{\text{OD (Control group)}} \times 100$$

2.8. Mitochondrial membrane potential detection

The mitochondrial membrane potential was detected using a JC-10 apoptosis detection kit purchased from KeyGEN. The cells were cultured for 1 day and 3 days under the treatment of MgAl-Cl and MgFe-NO₃ LDH. The cells were incubated with JC-10 working solution for 15 min at 37 °C in a 5% CO₂ incubator, and the fluorescence of FITC and PI was observed by a confocal fluorescence microscopy (Carl Zeiss).

2.9. Sequential changes of phagocytosis live-dead cell staining

The living and dead cell staining kit was purchased from Beyotime. hUC-MSCs were co-cultured with MgAl-Cl or MgFe-NO₃ LDH for 24 h and 48 h, respectively. The concentration of LDH nanoparticles was measured by gradient dilution method and set to 2.5, 5, 10, 20 and 40 $\mu\text{g}/\text{mL}$. The cells were collected by trypsin digestion and centrifugation and suspended in 400 μL of assay buffer. The cell suspension was added to 200 μL staining working solution and incubated at 37 °C for 15 min. Living (green fluorescence) and dead (red fluorescence) cells were detected using a confocal fluorescence microscope (Carl Zeiss).

2.10. hUC-MSC cell cycle detection

For cell cycle analysis, hUC-MSCs were seeded at $5 \times 10^4/\text{mL}$ in a 6-well plate, and the cells were treated with LDH (MgAl-Cl or MgFe-NO₃, 10 $\mu\text{g}/\text{mL}$) for 48 h. Then the cells were digested and dissociated into single cells with 0.25% ethylenediaminetetraacetic acid (EDTA) and placed in 70% cold ethanol at 4 °C overnight for 4 h. The cells were centrifuged (300 \times g, 5 min) and resuspended in a mixture of 100 μL RNaseA and 400 μL propidium iodide solution for 30 min. The cell cycle stage was detected immediately using flow cytometry. The cell cycle identification kit was purchased from KeyGEN.

2.11. Cellular uptake analysis

To detect the uptake efficiency of hUC-MSCs after LDH treatment, LDH was incubated 1:1 with FITC overnight one day in advance of the experiment. hUC-MSCs were cultured with MgAl-Cl or MgFe-NO₃ LDH for 0.5, 1, 2, 4, 6, 8, 24, and 48 h. Cellular uptake was evaluated using fluorescence-activated cell sorting (FACS) and confocal microscopy. For FACS analysis, cells in the 6-well plate were collected at defined times and transferred to a flow tube through a 200-mesh filter. The fluorescence intensity of FITC in each group was detected using flow cytometry. Blank cells were the control (Ctrl) group. For confocal analysis, cells in 24 well plates were collected after 24 h and processed as described above for immunofluorescence staining. The excitation wavelengths were 405 nm for DAPI, 488 nm for FITC, and 594 nm for both Lyso red used to label lysosomes and Mito red used to label mitochondria.

2.12. Animal model

An IVD needle puncture degeneration model was established in 8-week-old male Sprague-Dawley rats purchased from Tongji University (Shanghai, China). The procedures were approved by the ethics committee of Tongji Hospital affiliated with the Tongji University (ID: [2019] gxb-01). All surgical instruments were sterilized by autoclaving, and rats were anesthetized and placed at the intervertebral disc position

between S4–S5 on the caudal vertebra. After cutting the skin layer and exposing the intervertebral disc, a needle (20 g) puncture was conducted with at the depth 5 mm and rotated 360° for 15 s, which was approximately the distance that can penetrate the NP. The rats were randomly divided into sham, control, cell, and LDH groups. The rats in Sham group were only incised the outer layer of skin at the corresponding site without needle puncture. For cell and LDH group, hUC-MSCs were counted as 10^5 /mL and seeded in T75 Petri dish, and allowed for differentiation under control medium or MgFe-NO₃ LDH treated (10 µg/mL) differentiation medium for 7 days. After cell digestion, 10^6 cells were counted and placed in 10 µL in differentiation medium for each rat through a micro-needle injection 10 min after needle puncture. For Control group, 10 µL differentiation medium was injected into the defect area.

2.13. X ray and magnetic resonance imaging (MRI)

At 4, 8, and 12 weeks after surgery, three rats were randomly selected from each group for X-ray and MRI examinations. Each rat was placed in the supine position with its tail in a straight line on the molybdenum target radiation-imaging device. The exposure parameters of the X-ray machine (M – 20 X-ray-specific radiograph system; Faxtron, Tucson, AZ, USA) were set to 32 kV and 10 s duration. The disc height index (DHI) of the IVD in each group was calculated by dividing the disc height by the average of two adjacent vertebral body heights, and analyzed using the ImageJ software (NIH, Bethesda, MD, USA). MRI was performed using a Vero 1.5T system (Siemens, Munich, Germany). T2-weighted images were obtained on the coronal plane with the following parameters: visual field, 80 × 80 mm; slice thickness: 1.4 mm; repetition time, 4000 ms; echo time, 96 ms.

2.14. Histological analysis

IVD samples from each group were collected 12 weeks after the surgery. They were fixed with 4% PFA for 48 h in a 4 °C refrigerator. The solution was then replaced with EDTA decalcification solution once every 3 days. The decalcification effect was identified once a month until the IVD specimen was easily pierced using a needle. After decalcification, graded ethanol dehydration, xylene penetration, and paraffin embedding were performed. Sections (6 mm in thickness) were stained with hematoxylin and eosin (H&E) and Safranin O-fast green (S&O), and conducted with immunohistochemistry and immunofluorescence staining of COL1A1 (Cell Signaling Technology, CST, MA, USA), COL2A1 (Abcam), and Ki67 (Abcam).

2.15. Transcriptome sequencing and data analysis

Samples were divided into three groups: hUC-MSCs (undifferentiated cells), Ctrl, and LDH. The Ctrl and LDH groups were cultured for 7 days to permit chondrogenic differentiation of hUC-MSCs. Each group had three replicates. The cells were detached using trypsin, suspended to remove the supernatant, and stored in liquid nitrogen. RNA sequencing analysis was conducted at the Beijing Genomics Institute.

2.16. Wound healing analysis

To determine the lateral migration ability of hUC-MSCs co-cultured with MgFe-NO₃ LDH. According to the gradient dilution method, the material concentrations were 5, 10 and 20 µg/mL. Three replicates were used for the experimental group and the control groups [37]. First, a 2.5 µM live cell fluorescent probe CDCFCA (KeyGEN, China) was added to the medium and cultured in the dark for 30 min. Then, the cells were scraped with a 1 mL pipette on the edge of the ruler, and a straight line was drawn on the bottom of the cell culture plate. The cell fragments were gently washed off with PBS and replaced with prepared serum-free culture medium. Cell migration was observed and photographed using

an optical microscope (Olympus) at 0, 12, and 24 h after scratching. The cell migration indices were calculated using the ImageJ software as follows:

$$\text{Migration index (12 h)} = \frac{\text{Blank area (0 h)} - \text{Blank area (12 h)}}{\text{Blank area (0 h)}}$$

$$\text{Migration index (24 h)} = \frac{\text{Blank area (0 h)} - \text{Blank area (24 h)}}{\text{Blank area (0 h)}}$$

2.17. Transwell analysis of migration

To detect the longitudinal migration ability, 100 µL hUC-MSCs (2.5×10^5 /mL) were inoculated onto 8.0 µm Transwell inserts (Corning, New York, NY, USA). 1 mL MgFe-NO₃ solution with concentrations of 5, 10, and 20 µg/mL was added to the lower chamber of Transwell inserts. After 24 h, the cells in the upper inserts were gently wiped with a cotton swab. Cells in the lower chamber were fixed with 4% PFA for 10 min and stained with crystal violet (Beyotime) for 15 min. The cells were observed and photographed using a microscope. ImageJ software was used to count and compare the number of cells in each group.

2.18. Western blot analysis

The protein expression level of focal adhesion signaling pathway and downstream regulator factors were detected by western blot analysis. hUC-MSCs were counted as 2×10^5 /mL in a 6-well plate, treated with LDH (10 µg/mL), ATN (20 µM), and LDH (10 µg/mL) + ATN (20 µM) in the chondrogenic differentiation medium for 7 days differentiation. The cells were added with RIPA lysis buffer supplemented with protease inhibitor and PMSF to obtain the whole protein, and the protein count was quantified by BCA protein quantification kit (KeyGEN). The same amount of protein in each group was loaded for further detection. Primary antibodies including: COL1A1 (CST), Integrin (Abcam), Vinculin (Abcam), Actinin (CST), Akt (CST), p-Akt (CST), ERK (CST), p-ERK (CST), and β-Actin (Abcam).

2.19. Statistical analysis

The data are expressed as mean ± standard deviation (SD). All experiments were performed with at least three replicates. Statistical significance was estimated using one-way or two-way analysis of variance (ANOVA) within groups. The statistical differences are indicated as *p < 0.05, **p < 0.01, and ***p < 0.001.

3. Results

3.1. Characterization of LDH nanoparticles with different elemental composition

To screen the optimal nanoparticles, MgAl-Cl, MgFe-Cl, MgAl-NO₃ and MgFe-NO₃ LDH were synthesized. The internal lattice structures of the various LDH nanoparticles were observed using TEM. The TEM images indicated that the synthesized LDH nanoparticles were hexagonally layered with an average diameter of 100 nm (Fig. 1A). The elemental composition was analyzed by XPS in Fig. 1B, the data showed that MgAl-Cl LDH possessed Mg 1s (1303.6 eV), Al 2p (74.1 eV), Cl 2p (197.5 eV) elements, MgFe-Cl LDH possessed Mg 1s (1296.2 eV), Fe 2p (712 eV), Cl 2p (197.2 eV) elements, MgAl-NO₃ LDH possessed Mg 1s (1303.4 eV), Al 2p (73.9 eV), N 1s (406.5 eV), and O 1s (531.4 eV) elements, MgFe-NO₃ LDH possessed Mg 1s (1296.2 eV), Fe 2p (700.2 eV), N 1s (392.2 eV), and O 1s (525.2 eV) elements. XRD analysis was also performed to reveal the characteristic peaks in the four kinds of LDH (Fig. 1C). MgAl-Cl, MgFe-Cl, MgAl-NO₃, and MgFe-NO₃ LDH have typical (003), (006) and (009) diffraction peaks, and the 2θ angles of diffraction peak (003) in four LDH were 11.59°, 11.57°, 11.18°, and

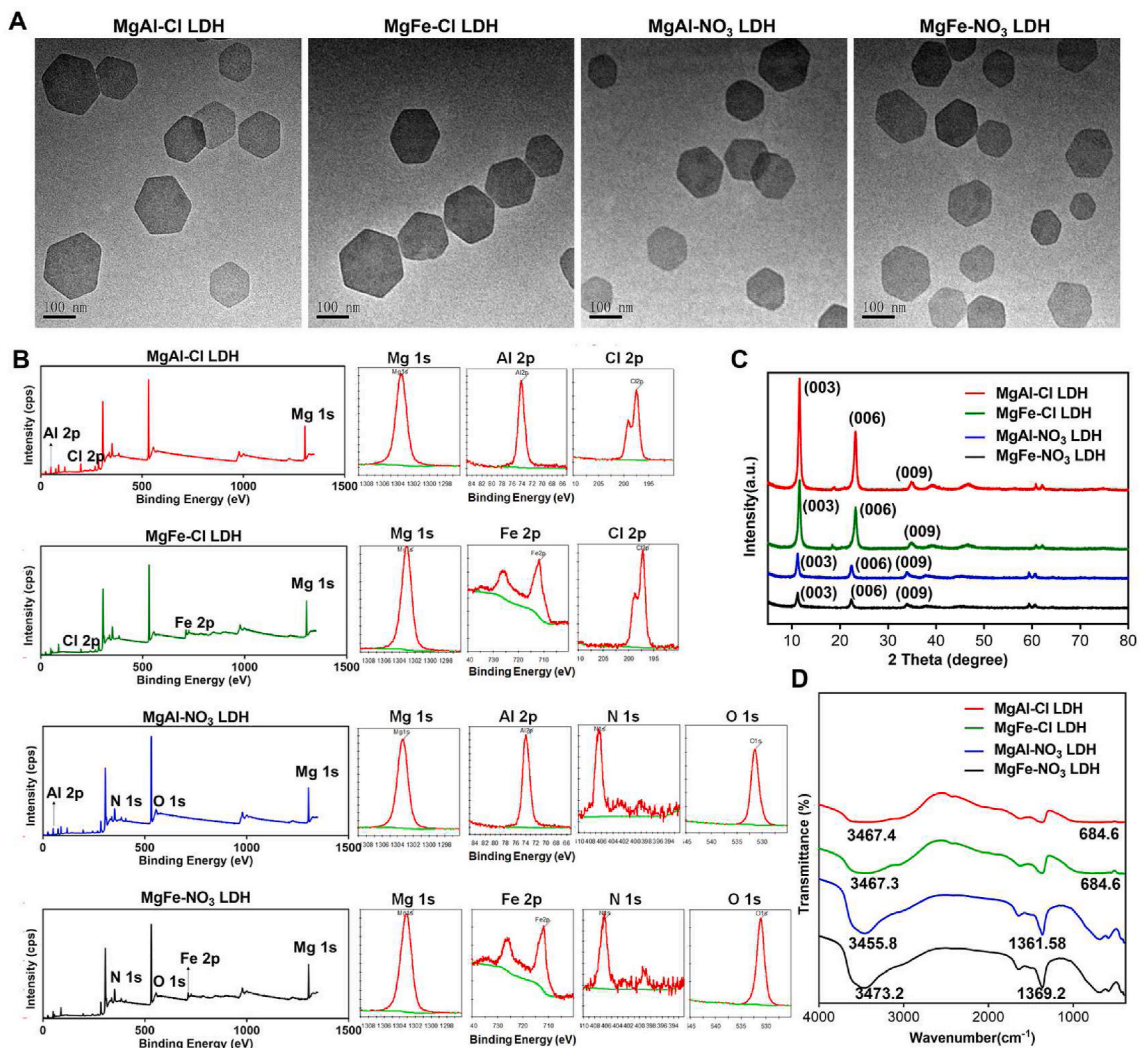


Fig. 1. The characterization of four types of LDH with different ion elements. A) TEM images of MgAl-Cl, MgFe-Cl, MgAl-NO₃ and MgFe-NO₃ LDH. Scale bar = 100 nm. B) XPS spectrum of elemental composition in MgAl-Cl, MgFe-Cl, MgAl-NO₃ and MgFe-NO₃ LDH. C) XRD analysis of MgAl-Cl, MgFe-Cl, MgAl-NO₃ and MgFe-NO₃ LDH. D) FTIR analysis of MgAl-Cl, MgFe-Cl, MgAl-NO₃ and MgFe-NO₃ LDH.

11.2°, respectively. According to the Bragg formula: $2d\sin(\theta) = n\lambda$, $n = 1$, $\lambda = 0.154$ nm, the values of crystal plane spacing d for four kinds of LDH were calculated as 0.762, 0.764, 0.791, and 0.789 nm, respectively. The positions of (003), (006) and (009) diffraction peaks for different LDH showed no obvious changes, which indicates that the metal ion and interlayer anion had no effects on the crystalline structure of LDH plate. From the LDH patterns of different metal element compositions, it can be seen that the intensities of the (003) and (006) diffraction peaks of the MgAl-Cl and MgFe-Cl LDH were significantly higher than those of the MgAl-NO₃ and MgFe-NO₃ LDH, indicating that the plate layer crystalline structures of MgAl-Cl and MgFe-Cl LDH were more obvious than those of MgAl-NO₃ and MgFe-NO₃ LDH, which is consistent with the previously reported results [37]. FTIR spectra (Fig. 1D) revealed representative OH⁻ vibrations at 3467.4, 3478.9, 3473.2, and 3475.1 cm⁻¹ in the MgAl-Cl, MgFe-Cl, MgAl-NO₃ and MgFe-NO₃ LDH, respectively. NO₃⁻ vibrations were evident at 1361.5 and 1369.2 cm⁻¹ in MgAl-NO₃ and MgFe-NO₃ LDH, respectively. C-Cl vibrations were evident at 684.6 cm⁻¹ in MgAl-Cl and MgFe-Cl LDH, respectively. In addition, the surface charge of the nanoparticles was measured. As shown in Fig. S1, the zeta potentials of the MgAl-Cl, MgFe-Cl, MgAl-NO₃, and MgFe-NO₃ LDH were +47.2, +40.6, +39.9, and +35.76 mV, respectively. These findings indicate the successful synthesis of LDH with different elemental compositions.

3.2. Chondrogenic promotive effects of different LDH nanoparticles

To further investigate the promoting effect of the different LDH preparations on chondrogenesis, hUC-MSCs were identified with negative and positive surface markers. The proportions of negative markers CD11b, CD14, CD45, and CD34 were 1.46%, 1.72%, 5.38%, and 1.83%, respectively (Fig. 2A). The proportion of positive markers CD29, CD73, CD44, CD166, and CD105 exceeded 95% (Fig. 2B). Then, the hUC-MSCs were co-cultured with 5, 10, 20, and 40 µg/mL of the different LDH nanoparticles for 10 and 14 days. As an initially marker of chondrogenic differentiation, glycosaminoglycan (GAG) deposition in hUC-MSCs was analyzed by Alcian blue staining, which is a common method for the qualitative detection of GAG in chondrocytes. As shown in Fig. 2C, blue GAG blue spots were observed in hUC-MSCs co-cultured with MgAl-Cl, MgFe-Cl, MgAl-NO₃, and MgFe-NO₃ LDH. Notably, the hUC-MSCs co-cultured with 20 and 40 µg/mL of MgAl-Cl and MgFe-NO₃ LDH groups stained dark blue. To better understand the chondrogenic promotive effect of LDH nanoparticles on MSCs, the expression of chondrogenic genes after 10 and 14 days was analyzed by RT-qPCR. SRY related HMG box-9 (Sox9) is expressed in chondrogenic progenitor cells and is a definitive marker of early stage chondrogenic differentiation. As shown in Fig. 2D, we measured the relative gene expression of SOX9 and COLX. After 10 days of culture, the expression of SOX9 and COLX in hUC-MSCs

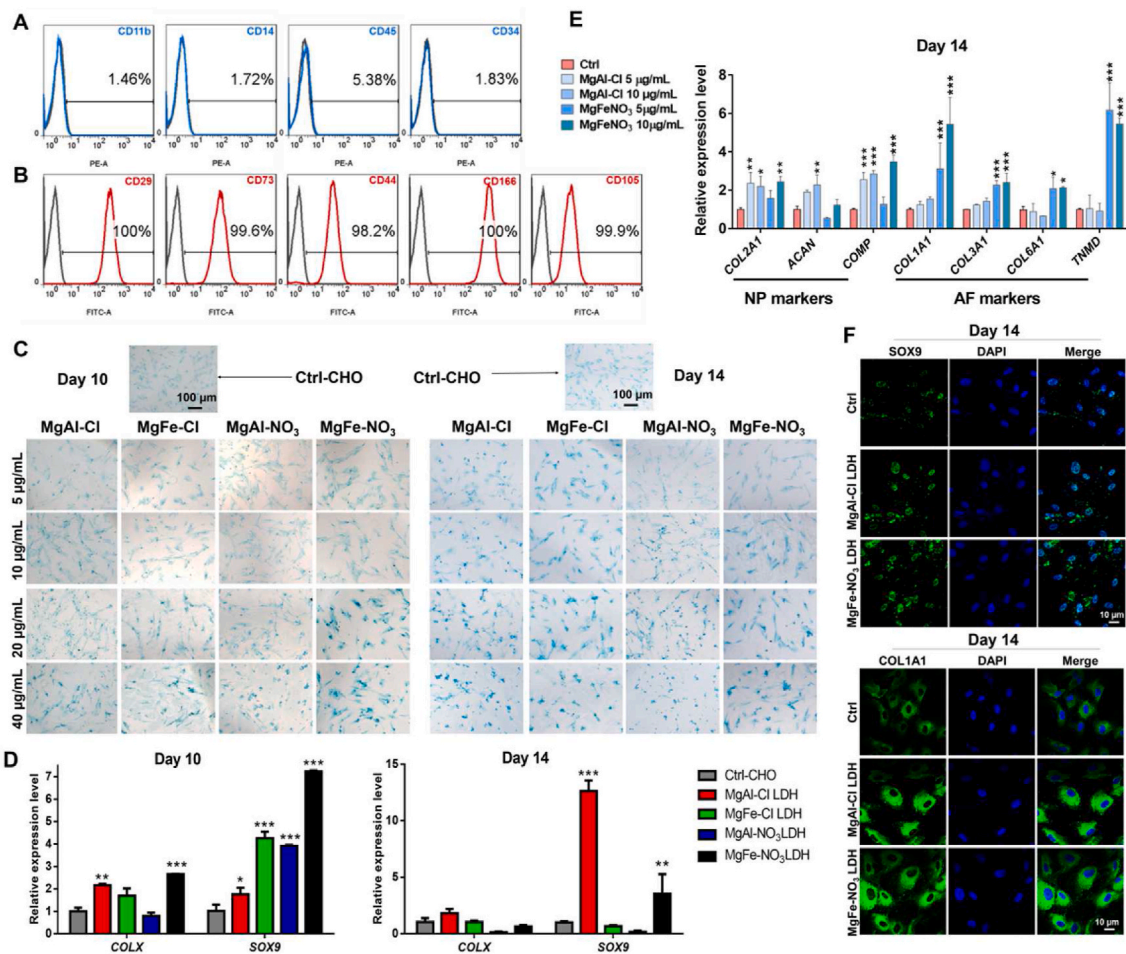


Fig. 2. The promoted chondrogenic differentiation of hUC-MSCs treated with different LDH nanoparticles. A) Negative surface markers identification of hUC-MSCs. B) Positive surface markers identification of hUC-MSCs. C) Alcian staining of hUC-MSCs for 10 days and 14 days chondrogenic differentiation. (Ctrl-CHO represents the control group for the same chondrogenic differentiation without adding LDH nanoparticles) Scale bar = 100 μm . D) qPCR analysis of total chondrogenic markers *COLX* and *SOX9* in LDH treated hUC-MSCs for 10 days and 14 days chondrogenic differentiation, respectively. * $p < 0.05$, ** $p < 0.01$, *** $p < 0.001$. E) qPCR analysis of NP marker genes *COL2A1*, *ACAN* and *COMP*, and AF marker genes *COL1A1*, *COL3A1*, *COL6A1* and *TNMD* expression under 5 $\mu\text{g}/\text{mL}$ and 10 $\mu\text{g}/\text{mL}$ MgAl-Cl and MgFe-NO₃ LDH treatment for 14 days. * $p < 0.05$, ** $p < 0.01$, *** $p < 0.001$. F) Immunofluorescence staining of SOX9 and COL1A1 in selected MgAl-Cl and MgFe-NO₃ LDH treated hUC-MSCs for 14 days chondrogenic differentiation. Scale bar = 10 μm .

co-cultured with MgAl-Cl and MgFe-NO₃ LDH was significantly higher than that of the other groups. After 14 days of culture, the expression of *SOX9* treated with MgAl-Cl LDH increased rapidly and that of MgFe-NO₃ LDH remained significantly higher than that of the other groups. Thus, we selected MgAl-Cl and MgFe-NO₃ LDH for further nanoparticle screening.

To investigate the specific hyaline-cartilaginous markers and fibrocartilaginous markers of MgAl-Cl and MgFe-NO₃ LDH nanoparticles, qPCR analysis and immunofluorescence were performed. As shown in Fig. 2E, we detected markers of NP and AF to evaluate the specific influence of MgAl-Cl and MgFe-NO₃ LDH at different concentrations, the results showed that 10 $\mu\text{g}/\text{mL}$ MgAl-Cl LDH could upregulate the expression level of NP markers *COL2A1*, *ACAN* and *COMP*, but showed little difference of AF markers. In addition, the treatment of MgFe-NO₃ LDH increased higher expression of AF markers *COL1A1*, *COL3A1*, *COL6A1* and *TNMD*. The protein expression of *SOX9* and *COL1A1* in hUC-MSCs was evaluated by confocal laser microscopy. After co-culturing with with MgAl-Cl LDH and MgFe-NO₃ LDH, MSCs showed much positive expression of *SOX9* and *COL1A1* compared with the control group after 14 days (Fig. 2F). These results indicated that both MgAl-Cl and MgFe-NO₃ LDH nanoparticles promoted the chondrogenesis of hUC-MSCs by up-regulating the chondrogenic genes.

3.3. Cytotoxicity evaluation and cellular uptake of MgAl-Cl and MgFe-NO₃ LDH nanoparticles in hUC-MSCs

The effects of MgAl-Cl and MgFe-NO₃ LDH nanoparticles on the proliferation and cytotoxicity of hUC-MSCs were evaluated using the CCK8 assay. As shown in Fig. 3A, the CCK8 assay demonstrated that MgFe-NO₃ LDH at concentrations of 1–40 $\mu\text{g}/\text{mL}$ co-cultured with hUC-MSCs for 1 day and 3 days exhibited no cytotoxicity. No significant differences in cell survival rates were observed between the control and hUC-MSCs co-cultured with different concentration of MgAl-Cl LDH for 1 day. However, when cells were treated with MgAl-Cl LDH for 3 days, the cell survival rate decreased in a dose-dependent manner. As shown in Figs. S2A and B, the intensity of EdU fluorescence revealed that cell proliferation barely changed in hUC-MSCs co-cultured with the two kinds of LDH nanoparticles compared to that in the control group. Consistently, live/dead staining results proved that MgFe-NO₃ LDH-treated hUC-MSCs preparations contained many more living cells than MgAl-Cl LDH-treated samples (Fig. S3). Cell cycle analysis showed that MgAl-Cl and MgFe-NO₃ LDH did not interfere with the inherent cell cycle distributions of the G1, S and G2 phases in hUC-MSCs (Fig. S4). These findings demonstrated the better compatibility of MgFe-NO₃ LDH than MgAl-Cl LDH.

To explore the cellular uptake difference between the two selected

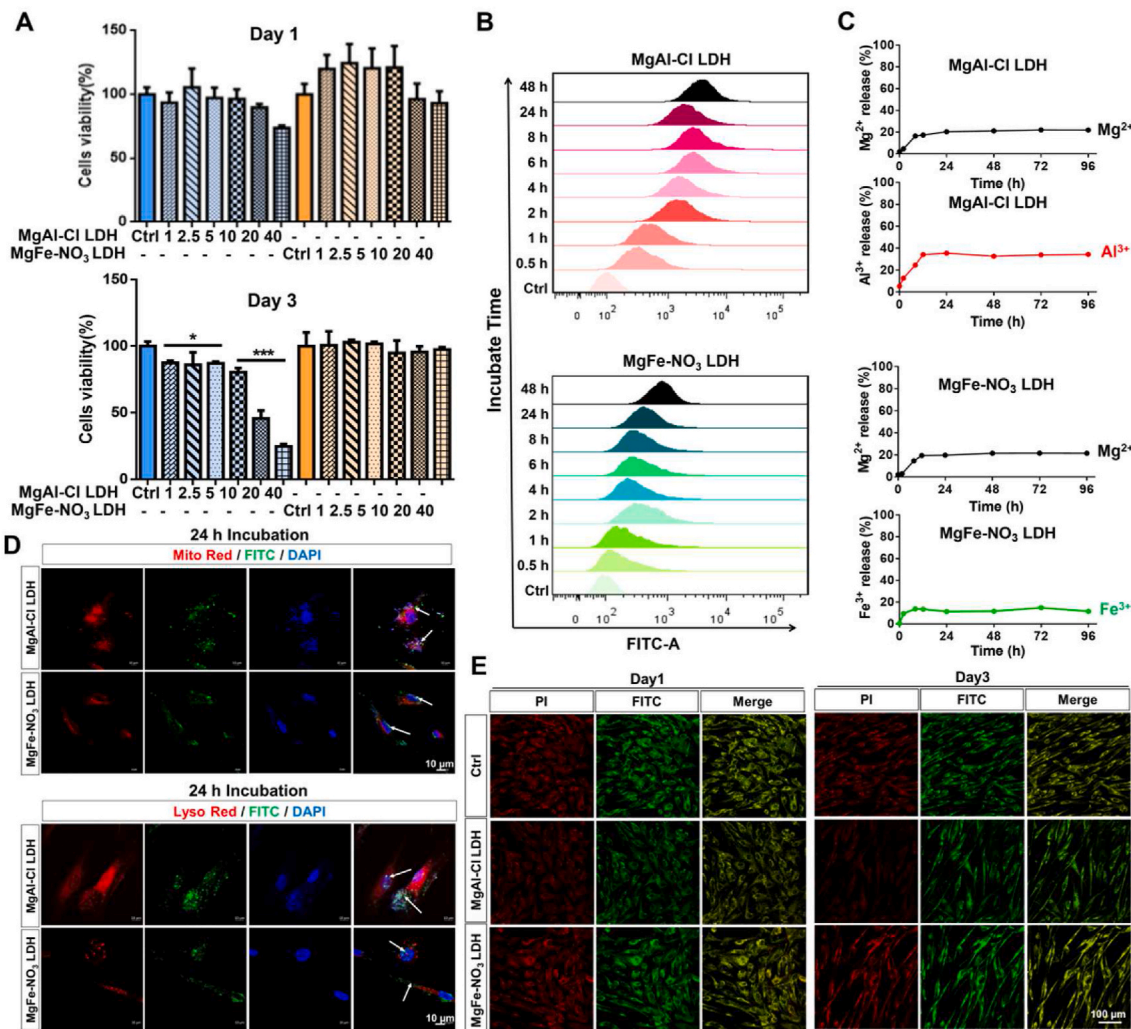


Fig. 3. The cell proliferation and cellular uptake of selected LDH nanoparticles in hUC-MSCs. A) CCK8 analysis of MgAl-Cl and MgFe-NO₃ LDH treated hUC-MSCs for 1 day and 3 days under different concentrations (1, 2.5, 5, 10, 20 and 40 μg/mL). **p* < 0.05, ****p* < 0.001. B) Flow cytometry analysis of cellular uptake of MgAl-Cl and MgFe-NO₃ LDH in hUC-MSCs after different time incubation (0.5, 1, 2, 4, 6, 8, 24 and 48 h). C) Metal ion release of MgAl-Cl LDH and MgFe-NO₃ LDH in PBS after different time. D) Immunofluorescence of cellular uptake of MgAl-Cl and MgFe-NO₃ LDH conjugated with FITC in hUC-MSCs after 24 h incubation, the organelle was labeled with mito-red (mitochondrial labeling, up) and lyso-red (lysosome labeling, down), respectively. Scale bar = 10 μm. E) Mitochondrial membrane potential of MgAl-Cl LDH and MgFe-NO₃ LDH treated hUC-MSCs for 1 day and 3 days. Scale bar = 100 μm.

LDH nanoparticles, hUC-MSCs were co-cultured with MgAl-Cl and MgFe-NO₃ LDH, which was linked with FITC for fluorescence labeling, and the cellular uptake was assessed by FACS for 0.5–48 h. Temporal phagocytosis of MgFe-NO₃ LDH by MSCs was analyzed using flow cytometry. As shown in Fig. 3B, FACS analysis revealed that FITC fluorescence appeared after 0.5 h incubation. The fluorescence intensity increased gradually with increasing co-culture time. A more positive FITC signal was observed in the MgAl-Cl LDH than in the MgFe-NO₃ LDH group, which might be responsible for the aggravated toxicity in Fig. 3A. As shown in Fig. 3C, the release of divalent and trivalent metal ions was stable after 24 h, and the maximum Mg²⁺ release of MgAl-Cl LDH and MgFe-NO₃ LDH was similar at 21.9% and 21.5%, while the maximum Al³⁺ and Fe³⁺ release showed significant difference at 34.4% and 14.9%, respectively. Thus, the results could explain the superior biocompatibility of MgFe-NO₃ than MgAl-Cl LDH. To verify the results of FACS, confocal analysis was performed. The results of 24 h incubation showed that most of the MgAl-Cl LDH accumulations overlapped with organelles of mitochondria and lysosomes, while only some inconspicuous signal spots were observed in the MgFe-NO₃ LDH-treated MSCs (Fig. 3D). Moreover, we detected the mitochondrial membrane potential by JC-10 and conducted immunofluorescence analysis to observe the

fluorescent expression of PI and FITC in each group using JC-10 in Fig. 3E. The results showed that MgAl-Cl LDH and MgFe-NO₃ LDH-treated hUC-MSCs for 1 day did not influence the mitochondrial membrane potential compared with Control group. While, after MgAl-Cl LDH treatment for 3 days, hUC-MSCs showed significant FITC fluorescent decrease, indicating that JC-10 selectively enters mitochondria and undergoes a reversible change in color from green to orange due to an increase in membrane potential. And MgFe-NO₃ LDH showed a comparable mitochondrial potential without fluorescent expression changes after 3 days treatment. Considering the efficiency of chondrogenic differentiation promotion and cytotoxicity, MgFe-NO₃ LDH was judged as the optimal material for further *in vivo* research.

3.4. *In situ* IVD regeneration effects of MgFe-NO₃ LDH-pretreated hUC-MSCs transplantation

To detect the effects of LDH-treated hUC-MSCs transplantation on *in vivo* IDD regeneration, a rat IVD injury model was established by needle puncture (Fig. 4A and B). hUC-MSCs were co-cultured with or without the optimizing MgFe-NO₃ LDH for 7 days in chondrogenic differentiation medium. Then, cells were counted and transplanted into the injury

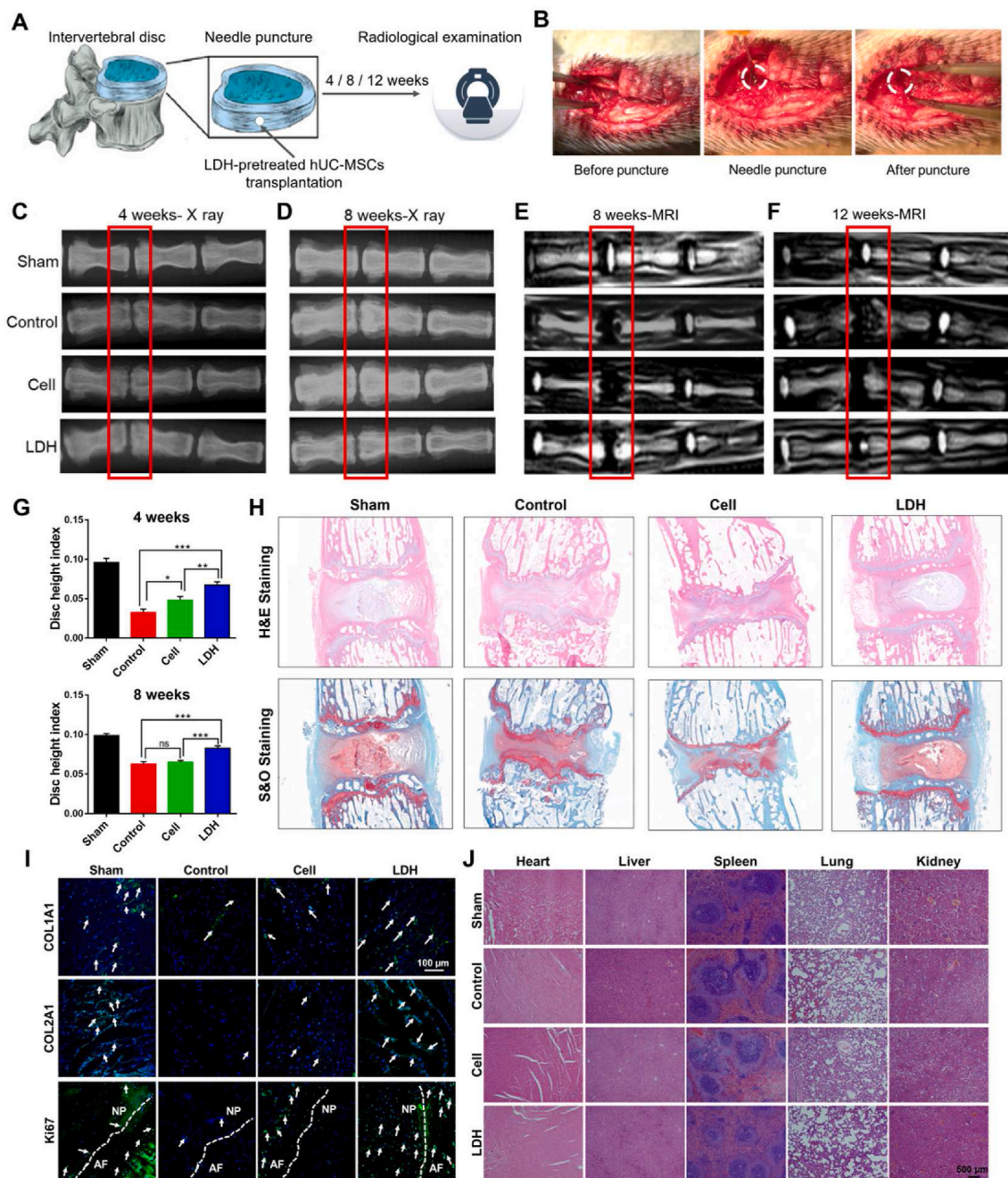


Fig. 4. The *in situ* IVD regeneration function of optimizing LDH pretreated hUC-MSCs for 7 days chondrogenic differentiation and transplantation in the injury site of rat model. A) The schematic diagram of IDD model constructed by needle puncture. B) The photo records of surgical model construction. C) X-ray analysis of IVD height change with different treatment after 4 weeks. D) X-ray analysis after 8 weeks. E) MRI analysis after 8 weeks. F) MRI analysis after 12 weeks. G) The disc height index (DHI) of optimizing LDH-pretreated cell transplantation effects 4 weeks and 8 weeks after surgery. * $p < 0.05$, ** $p < 0.01$, *** $p < 0.001$. H) H&E and S&O staining of different treatment after 12 weeks. I) Immunofluorescent of COL1A1, COL2A1 and Ki67 staining of different treatment after 12 weeks. White arrows indicate positive cells. Scale bar = 100 μm . J) Tissue H&E staining of main organs including heart, liver, spleen, lung and kidney in Sham, Control, Cell and LDH groups after 12 weeks operation. Scale bar = 500 μm .

site. The sham rats and control groups were set as positive and negative controls, respectively, for further radiography and histology studies. The degenerative discs were thinned by herniated NP, exhibited reduced disc water content, and had reduced space. The Degenerative discs are thinned by herniated nucleus pulposus (NP) and reduced disc water content, thus presenting as reduced space. X-ray images showed that significant disc space narrowing at 4 and 8 weeks after the induction of IVD degeneration in the control group. The effects in cells without LDH treatment were similar to those in the control group, but the progress was relatively slow (Fig. 4C and D). Radiological analysis was used to

detect the DHI at 4 and 8 weeks after LDH-treated MSC transplantation (Fig. 4G). Notably, the DHI of the LDH-treated MSC transplantation group was almost the same as that of the sham group. A decrease in disc height occurs with a decrease in water content, which is associated with a reduction in proteoglycans. The high signal intensity of T2-weighted images in MRI is commonly utilized to assess water content in the IVD. A lower signal indicates atrophy and dehydration. In the present study, at the late stage of degeneration in the control group, the stability of the IVD decreased, the morphology changed, and the signal of NP in T2-weighted images were decreased and showed a “black disc”

appearance after complete degeneration (Fig. 4E and F).

As shown in Fig. 4F, at 12 weeks after LDH-treated MSCs transplantation, there was high signal intensity at the injury site of IVD, indicating the presence of new cartilage-like tissues. However, the control and non-LDH-treated MSC groups did not show high signal intensity. Furthermore, histology was evaluated using H&E and S&O stainings. As shown in Fig. 4H, both stains produced a similar staining pattern in LDH-treated MSC and sham groups. The X-ray, MRI, and histological results indicated that transplantation of LDH-treated MSCs effectively led to IVD regeneration. The data showed successful establishment of IDD model histologically. And immunofluorescent and immunohistological analyses of tissue samples in Sham, Control, Cell and LDH group to reveal the COL1A1 and COL2A1 expression in Fig. 4I and Fig. S5. The results indicated that LDH group have more positive COL1A1 cells in AF, COL2A1 cells in NP, and Ki67 positive cells in AF

and NP.

In order to detect the degradability of LDH, we conducted an *in vivo* imaging analysis to investigated the degradation of LDH particles bonded with Cy5.5. The data showed that after LDH-Cy5.5 injection, the fluorescence gradually increased from 2 h to 8 h, and decreased from 24 h to 48 h at a very low level, which indicate the basically degradation of LDH nanoparticles (Fig. S6). In addition, the H&E staining in Fig. 4J clearly demonstrated the implantation of cells or LDH-pretreated cells did not cause tissue toxicity in rats. The above results indicated that LDH could stimulate cell proliferation in the defective disc, thus promoting chondrogenic differentiation for tissue regeneration.

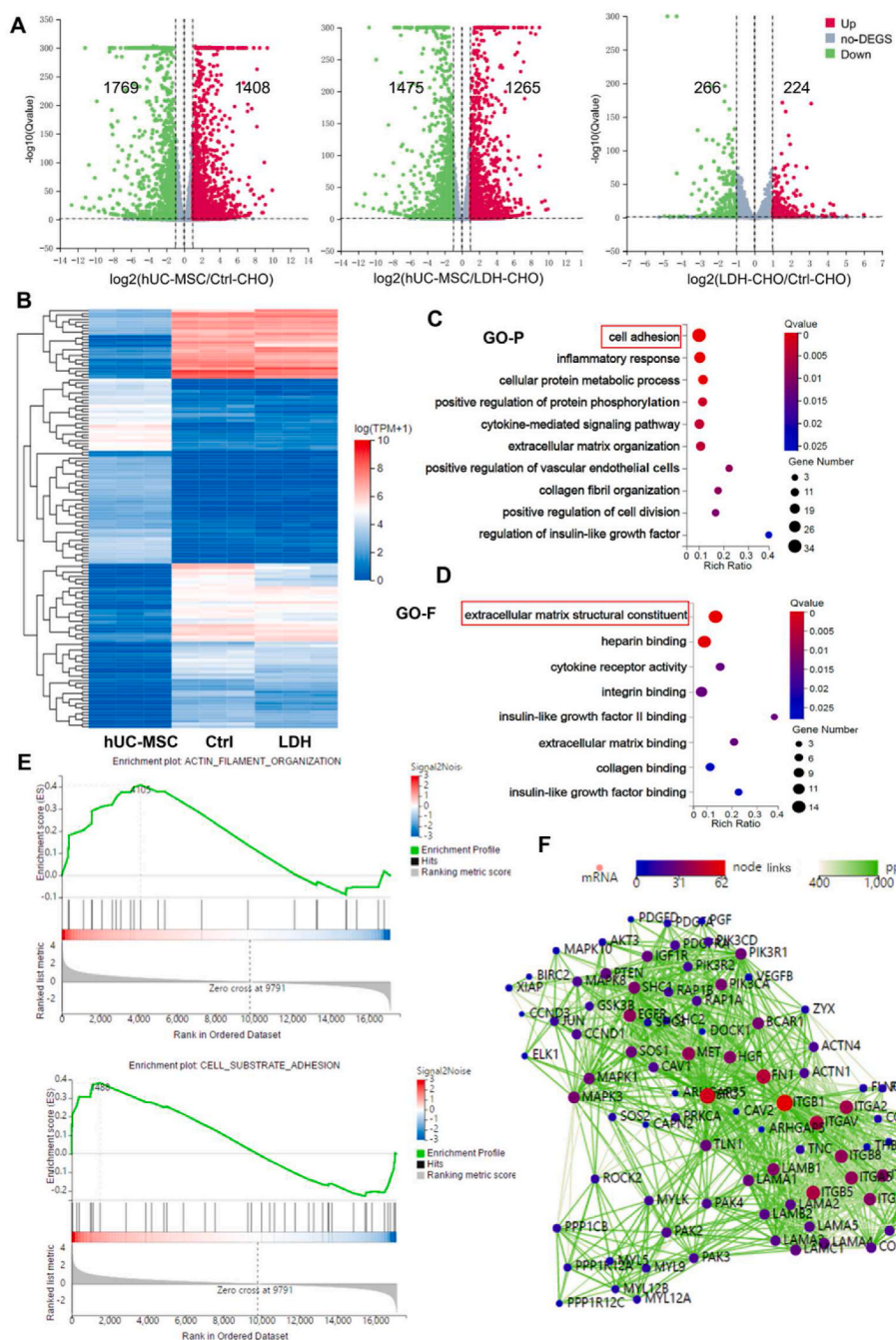


Fig. 5. Transcriptome profiling of optimized LDH-regulated hUC-MSC function and mechanism. A) The volcano diagram of hUC-MSC (undifferentiated control group), Ctrl-CHO (differentiation control group) and LDH group. B) The heatmap distribution of hUC-MSCs, Ctrl and LDH treated groups. C) GO-P bubble graph of LDH regulated differentially expressed genes (DEGs). D) GO-F analysis of LDH regulated DEGs. E) GSEA analysis of ACTIN filament organization and cell substrate adhesion. F) Protein-protein-interactions (PPI) analysis of LDH regulated significant genes.

3.5. Transcriptional profiling of optimized LDH regulating hUC-MSC function

To reveal the potential molecular mechanisms by which MgFe-NO₃ LDH promotes IVD regeneration, the transcriptomes of LDH-treated MSCs were examined using RNA sequencing. Volcano plots revealed differentially expressed genes (DEGs) between the treated groups (Fig. 5A). There were 1408 upregulated and 1769 downregulated genes in Ctrl-CHO vs. hUC-MSCs, 1265 upregulated and 1475 downregulated genes in LDH-CHO vs. hUC-MSCs, and 224 upregulated and 266 downregulated genes in Ctrl-CHO vs. LDH-CHO ($p < 0.05$, log₂ fold change > 1). Fig. 5B presents a cluster heatmap of the 124 most significant DEGs among the sample groups ($p < 0.05$ and log₂ fold change > 2). Gene ontology (GO) analysis was performed to more thoroughly investigate the signaling pathways involved in the IVD regeneration of LDH-treated MSCs. The GO analysis was classified into two categories: GO-P (biological process of selected genes) and GO-F (molecular function of the gene products). DEGs between the LDH and the Ctrl-CHO groups were mainly associated with cell adhesion, inflammatory response, angiogenesis, and cellular protein metabolic processes (Fig. 5C and D). GO-F mainly contains molecular functions associated with ECM structural constituents, heparin binding and cell adhesion-related genes, which were significantly different between the MgFe-NO₃ LDH-treated

and control groups, suggesting that optimization of LDH could regulate the constituents of ECM and promote cell migration. Transcriptome sequencing data showed that focal adhesion signaling pathway plays a key role in promoting chondrogenic differentiation of hUC-MSCs by MgFe-NO₃ LDH. The Integrin gene was significantly altered in both gene set enrichment analysis (GSEA) of cell adhesion and actin cytoskeleton function (Fig. 5E). Protein-protein-interactions analysis was performed to evaluate the key gene of LDH regulation in hUC-MSCs. The findings clearly indicated the multiple links of the integrin family with chondrogenic genes and ECM components (Fig. 5F). The collective transcriptomic data identified ECM structural constituents and cell adhesion pathways as highly enriched terms that facilitated our further functional intervention.

3.6. Cellular adhesion and migration ability of LDH-treated hUC-MSCs

To explore the molecular mechanism by which MgFe-NO₃ LDH promotes MSCs migration, the expression of focal adhesion-related genes, including α -Actinin, *Integrin* and *Cdc42*, was analyzed by RT-PCR. The relative expressions of α -Actinin and *Integrin* in LDH-treated MSCs was significantly higher than that in other groups. However, no significant differences were found in *Cdc42* expression in all groups, suggesting that LDH promoted the migration of MSCs by regulating focal

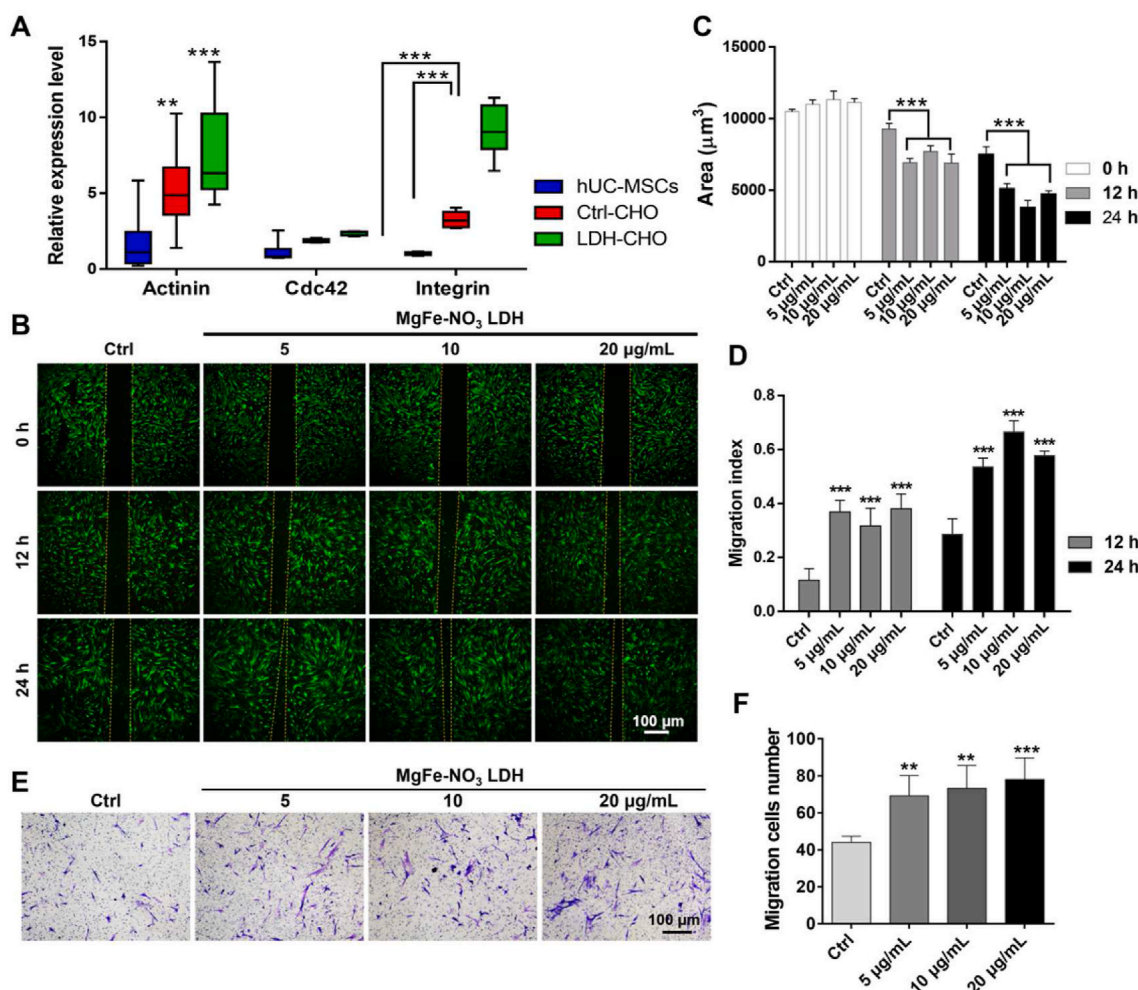


Fig. 6. The cell adhesion and migration ability of optimizing LDH in regulating hUC-MSCs function. A) qPCR analysis of focal adhesion signaling pathway related markers *Actinin*, *Cdc42* and *Integrin* expression. ** $p < 0.01$, *** $p < 0.001$. B) Wound healing analysis of cell adhesion ability in optimizing LDH treated hUC-MSCs for 12 h and 24 h, respectively. Scale bar = 100 µm. C) Blank area calculation of figure B quantified by image J. *** $p < 0.001$. D) Migration index calculation of figure B of 12 h and 24 h. *** $p < 0.001$. E) Cell migration analysis detected by crystal violet. Scale bar = 100 µm. F) Migration cells number in figure E quantified by image J. ** $p < 0.01$, *** $p < 0.001$.

adhesion-related genes (Fig. 6A). Based on the transcriptomic analysis of LDH-treated MSCs, the effect of MgFe-NO₃ LDH on the migration ability of MSCs was tested by performing wound healing and Transwell assays. hUC-MSCs were co-cultured with 5, 10, and 20 μg/mL MgFe-NO₃ LDH for 12 and 24 h. As shown in Fig. 6B–D, the migration ability of LDH-treated MSCs was approximately 3- and 2-folds, respectively, compared to that of control group after 12 and 24 h of treatment. The narrowed gap in Fig. 6B was measured using the Image J software. LDH-treated MSCs displayed a narrower gap than the control group. As shown in Fig. 6E and F, addition of MgFe-NO₃ LDH considerably showed concentration dependent promotion effects of cell migration.

3.7. Inhibition of integrin in focal adhesion signaling pathway impaires LDH-promoted differentiation and migration of MSCs

Based on the above functional validation of the optimized MgFe-NO₃ LDH on cell adhesion and migration ability *in vitro*, we next explored the

effect of inhibiting the integrin pathway by transcriptome analysis and qPCR validation. The pathway is of crucial rule in the focal adhesion signaling pathway that mediates the recognition between cells and the ECM. To further clarify the underlying mechanism, MSCs were co-cultured with MgFe-NO₃ LDH and the focal adhesion pathway inhibitor ATN (Fig. 7A), and the results showed that the most effective concentration of ATN was 20 μM. The migration ability of MSCs was still tested by wound healing, as shown in Fig. 7B and C, MgFe-NO₃ LDH could no longer promote the migration of MSCs in the presence of ATN. As shown in Fig. 7D, the fluorescence intensity of Integrin and SOX9 was the highest in the MgFe-NO₃ treatment group, and the cell morphology of F-Actin was significantly widened and enlarged. After the addition of ATN, the fluorescence intensity of Integrin and SOX9 decreased in the ATN group, and the cell morphology of F-Actin decreased significantly. The findings indicate that the addition of ATN significantly inhibited chondroblast differentiation and the ability of cell migration and adhesion. In the LDH + ATN group, the yellow fluorescence intensity of

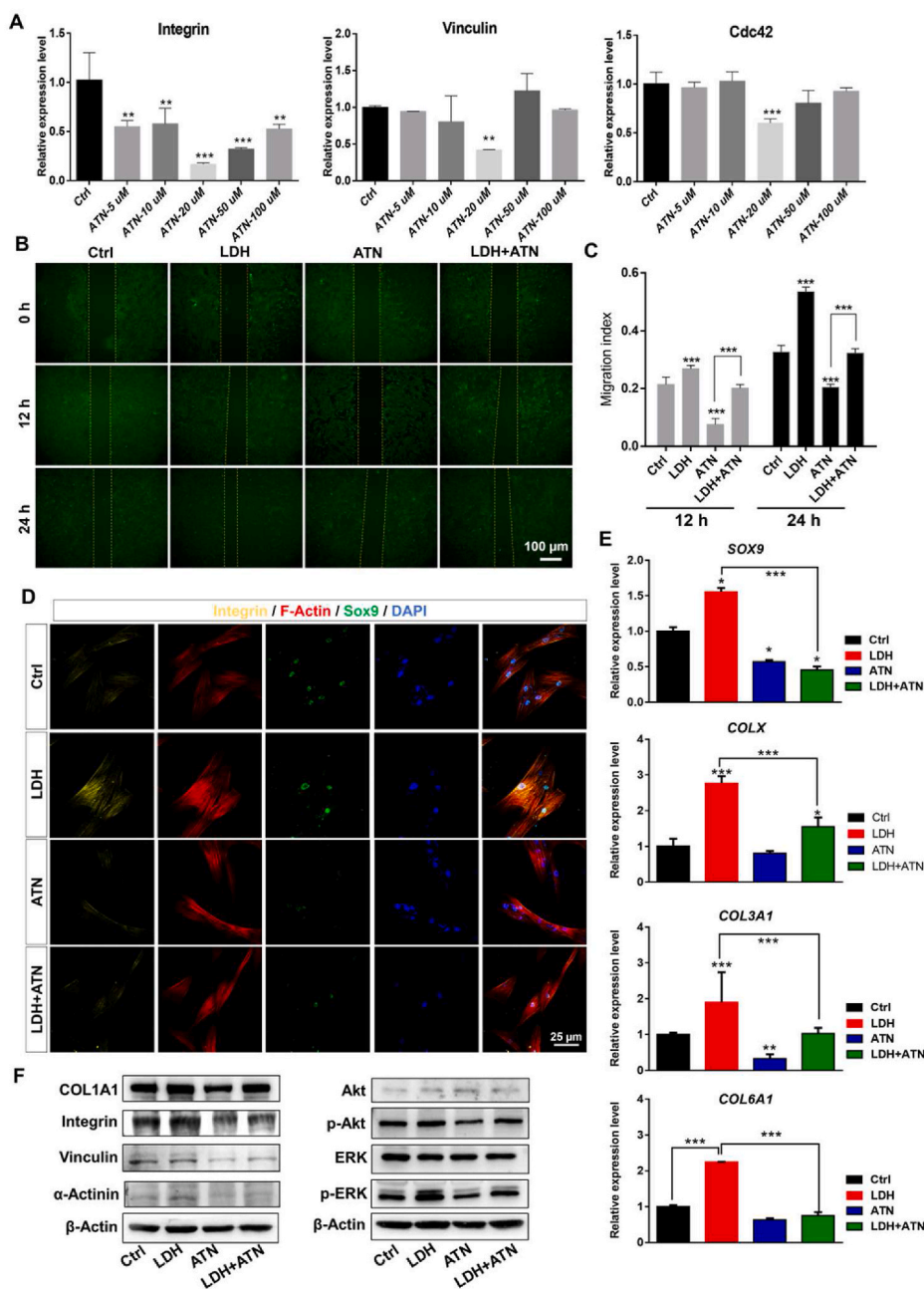


Fig. 7. Focal adhesion signaling pathway validation of optimizing LDH regulated hUC-MSCs toward chondrogenic differentiation. A) qPCR analysis of focal adhesion signaling pathways markers *Integrin*, *Vinculin* and *Cdc42* under different concentrations of integrin inhibitor ATN (5, 10, 20, 50 and 100 μM, respectively). **p < 0.01, ***p < 0.001. Scale bar = 100 μm. B) Cell migration detect of LDH, ATN and LDH + ATN groups. C) The migration index of figure B quantified by image J. ***p < 0.001. D) Immunofluorescence of LDH, ATN and LDH + ATN treated hUC-MSCs for 7 days chondrogenic differentiation. Scale bar = 25 μm. E) qPCR analysis of chondrogenic markers *SOX9*, *COLX*, *COL3A1* and *COL6A1* expression. *p < 0.05, ***p < 0.001. F) Western blot analysis of focal adhesion related proteins after the treatment of LDH, ATN and LDH + ATN for 7 days chondrogenic differentiation.

Integrin and the green fluorescence intensity of SOX9 were increased compared to that in the ATN group. The morphology of the Actin cytoskeleton was also significantly widened. The results showed that the addition of ATN effectively inhibited the differentiation, migration, and adhesion of hUC-MSCs and that MgFe-NO₃ LDH promoted chondrogenic differentiation, cell migration, and adhesion of hUC-MSCs in the presence of ATN. We further evaluated the colocalization of LDH with the cell membrane labeled with the lipophilic fluorescent dye DiI. The results showed that with the increase in LDH incubation time, the colocalization of LDH was augmented from 0.5 to 48 h (Fig. S7A). The cell skeletal Actin fluorescence shown in Fig. S7B indicated that LDH incubation could enhance the intensity of Actin, leading to a downstream regulatory reaction. qPCR was also conducted in LDH-, ATN-, and LDH + ATN-treated hUC-MSCs for 7 days of chondrogenic differentiation. The downregulation of ATN reduced total chondrogenic genes (SOX9 and COLX) and fibrocartilaginous genes (COL1A1 and COL3A1). The findings were highly consistent with the immunofluorescence results and indicate that the chondrogenic promoting function of LDH could be compromised by ATN co-treatment in the LDH + ATN group (Fig. 7E). Western blot analysis of focal adhesion signaling pathways in Fig. 7F clearly demonstrated the promoting effects of Integrin, Vinculin and α -Actinin treated by LDH, and the effective upregulation of p-Akt and p-ERK indicated a possible correlation between focal adhesion signaling pathway with PI3K-Akt signaling pathway and MAPK

signaling pathway. In addition, we conducted immunofluorescent analysis of Vinculin after LDH, ATN and LDH + ATN treatment in Fig. S8, the data showed that consistent with immunofluorescence of Integrin, the ATN adding could significantly decrease the expression of Vinculin. The above results demonstrated that optimizing LDH has a significant influence on chondrogenic function by regulating the key genes of Integrin and downstream gene Vinculin in the focal adhesion signaling pathway.

The *in vivo* transplantation effects of hUC-MSCs for chondrogenic differentiation with or without LDH treatment support the following sequence of events for the optimizing LDH function. Without LDH treatment, the intervertebral disc was characterized of reduced disc height, destroyed structure, and loss of physiological function. While, LDH first produces ECM components and then interacts with the integrin receptor of focal adhesion signaling pathway. This induces the upregulation of downstream markers of focal adhesion kinase Vinculin, Actinin and Cdc42 expression, supplemented with the regulation of p-Akt and p-ERK, facilitating the regulation of actin skeletal distribution and assembly, and the ultimate chondrogenic differentiation of transcription factor SOX9 and collagen components COLX, COL1A1, COL3A1, and COL6A1 (Fig. 8).

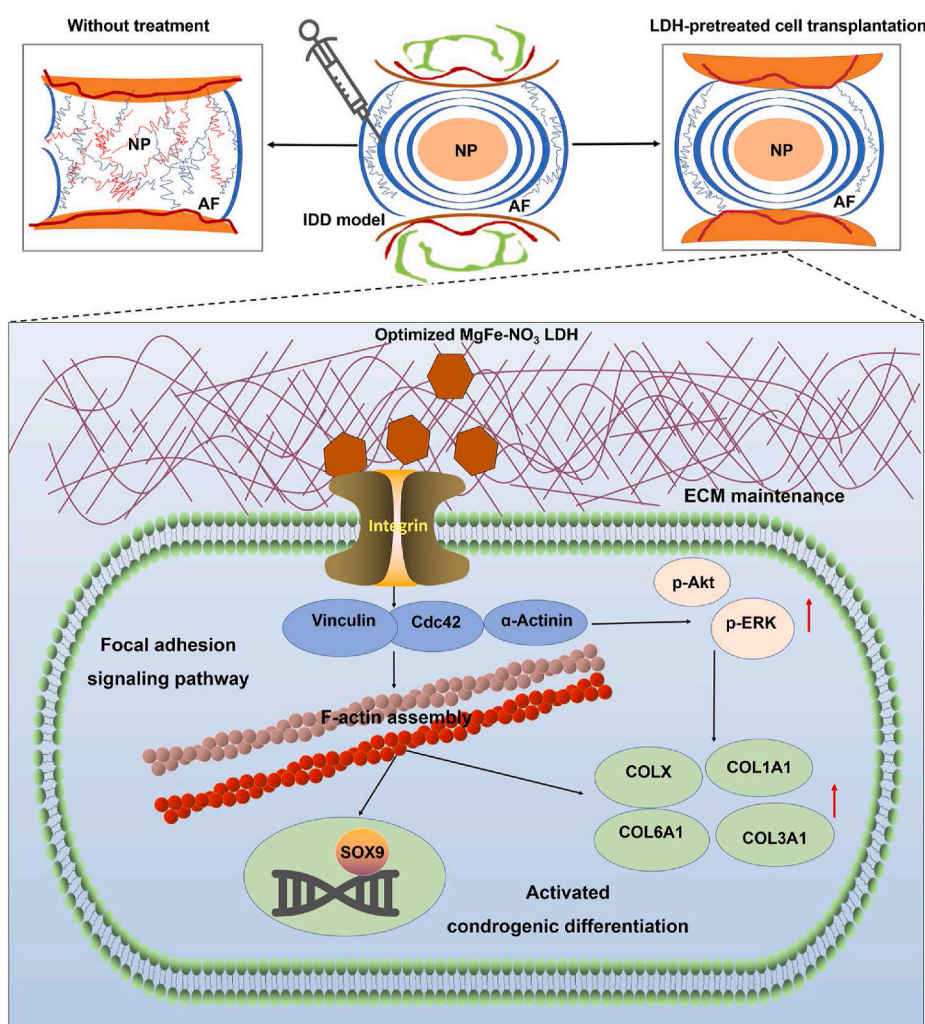


Fig. 8. Schematic diagram of the function and mechanism of IDD model with or without LDH treatment. Without LDH treatment, the intervertebral disc was characterized of reduced disc height, destroyed structure, and loss of physiological function. While, the optimized LDH-pretreated cell transplantation enhanced the chondrogenic differentiation and *in situ* intervertebral disc regeneration through focal adhesion signaling pathways.

4. Discussion

The structural characteristics of IVD mainly support the motor function and stability of the spine [38,39]. IVD degeneration often affects the facet joints at the back of the spine and is a common cause of back pain [40]. Current treatments for disc degeneration can be divided into conservative treatment and surgery. When conservative treatment methods, such as physical therapy, drug treatment, and epidural steroid injection fail, surgical intervention involving vertebral fusion is needed to reduce pain and other symptoms by limiting the movement of the diseased segment of the vertebral body [8,10]. However, the decreased activity of the vertebral body will accelerate the degenerative changes of the adjacent disc [9,41].

The use of stem cells to treat discs degeneration *in vitro* and *in vivo* has continued to progress and several clinical trials have been conducted to evaluate the treatment efficacy and safety [17,42]. Biomaterials are often applied in conjunction with stem cell transplantation in the treatment of IDD. These biomaterials are most often biological scaffolds that are intended to provide microenvironment support for transplanted stem cells and ensure the stability of their cell morphology and function [43,44]. However, reflecting their original goal of physical support, biomaterial scaffolds display poor environmental interaction and cannot accurately regulate stem cell differentiation [18,19]. In this study, we screened the optimal LDH materials according to the differentiation ability and characteristics of stem cells, co-culture ability, and synergistically evaluated the mechanism of LDH-treated hUC-MSCs function and process. This study aimed to provide new ideas and regeneration intervention methods for tissue engineering.

Mg-based materials exhibit excellent biocompatibility applications [45]. We constructed four Mg-based LDHs composed of different trivalent ions and negative ions based on the co-precipitation and hydrothermal method [46,47], which were characterized by TEM, surface zeta potential, XRD, XPS and FTIR analyses (Fig. 1A–D). The results indicated excellent layered structures and homogeneous distribution of the nanoparticles [48]. The positive surface zeta potential facilitated LDH for cell adhesion and endocytosis into the targeted cells [49]. The ion elemental composition of LDH has been reported as functional roles in directing the stem cell fate at different stages and culture systems [35]. Thus, the ion-elemental specific LDH provides promising insights for controlling stem cell fate.

The four LDH nanoparticles were evaluated by Alcian staining, qPCR, and immunofluorescence after co-culturing with hUC-MSCs. MgAl-Cl and MgFe-NO₃ LDH displayed better chondrogenic differentiation effects than the others tested (Fig. 2A–C). The different expression levels of SOX9 between day 10 and 14 mainly because of the expression pattern of the gene and the regulation transition of LDH treatment. We added specific evaluation of NP markers and AF markers to more clearly investigate the function of MgAl-Cl and MgFe-NO₃ LDH, and we also conducted immunofluorescence analysis of COL1A1 to prove the function model of fibrocartilage marker. GAG is a recognized chondrocyte component and is one of the most typical products of cartilage [50]. In the present study, GAG was stained intensively, and its number visibly increased in MSCs with an increase in LDH nanoparticles. In addition, compared with the other groups, MgAl-Cl and MgFe-NO₃ LDH treated hUC-MSCs displayed higher cell density and more regular cell morphology. Cell viability analysis by CCK8 as well as EdU and cellular distribution experiments revealed MgFe-NO₃ LDH as the most favorable material, with relatively higher efficiency in promoting chondrogenesis and cell compatibility, which is important for the *in vivo* regeneration of IVD [51–53].

Earlier studies demonstrated the feasibility of transplantation of MSCs [18,54]. Based on the advantages of LDH and MSCs in tissue regeneration and microenvironment regulation, the combined application of LDH and MSCs should bring exciting results for tissue regeneration and repair therapy. In this study, we constructed LDH pre-treated MSCs and then transplanted them into the degenerative site of a needle

puncture degenerative disease rat model. The *in vivo* findings clearly showed recovery of disc space height and integrated tissue structure similar to that of the native IVD (Fig. 4). Thus, transplantation of LDH-treated MSCs could effectively promote chondrogenesis. New cartilage with obvious morphology was evident compared with the untreated MSCs group. By exploring the specific mechanisms of related intervention pathways in the process of regeneration and repair, the good proliferation and differentiation potential of stem cells can be fully utilized.

To reveal the molecular mechanism of LDH-promoted chondrogenic differentiation of MSCs, transcriptional profiling was performed. Cell adhesion and ECM components were significantly affected (Fig. 5C–F). The key gene was integrin, which plays a crucial role in the focal adhesion signaling pathway that mediates cell adhesion and recognition between cells and ECM as evident through transcriptome analysis and qPCR validation (Fig. 6A). The focal adhesion signaling pathway may have important roles in cellular motility, bone phylogeny, and cell growth and differentiation related pathways [55,56]. Our results are consistent with those of published reports on the function of Integrin and the expression trend of chondrogenic differentiation (Fig. 7D). To verify that LDH promoted chondrogenic differentiation of MSCs by inhibiting the focal adhesion signaling pathway and thus contributing to chondrogenesis, we inhibited the Integrin expression by small molecules in LDH-treated MSCs cells (Fig. 7E and F). Notably, the chondrogenic activity of LDH was significantly reduced. The results identify the molecular mechanism and prove that focal adhesion signaling pathway is crucial in promoting the chondrogenic differentiation of LDH-treated MSCs.

Focal adhesion signaling pathway mainly contain the physical connection between the ECM and the actin cytoskeleton of the cell [57]. The preliminary function was exerted through integrins, which were commonly found dependent on Ca²⁺ or Mg²⁺. Integrins also have a role in transmitting extracellular signals into the cell [58]. The extracellular structural domains of integrins bind to extracellular ligands resulting in a cascade reaction of signal amplification [59]. Vinculin is involved in cellular chemical signaling by binding and interacting with a variety of adhesion site proteins via integrins [60]. Studies have demonstrated F-actin parallels with the change of Vinculin in the synthesis of collagen ECM and the remodelling of cytoskeleton-ECM adhesion in chondrogenic differentiation of MSCs [61,62]. Focal adhesion kinase (FAK) can integrate signals from integrins, growth factors and mechanical stimuli to activate intracellular PI3K/Akt, Ras/MAPK and other signaling pathways to regulate cell growth [62,63]. Our results showed that LDH promoted the Integrin, Vinculin, Actinin expression, and upregulated the expression of p-Akt and p-ERK correspondingly (Fig. 7D–F). Consistent with earlier reports, our findings indicate the involvement of PI3K/Akt and Ras/MAPK in focal adhesion signaling pathway.

The adhesion ability of ECM is very important for the proliferation, survival, differentiation, and differentiation of MSCs [64]. ECM simulates the structure of natural osteochondral tissue, increases cell adhesion ability, and provides a more favorable matrix for IVD regeneration [65]. Furthermore, ECM can effectively mimic the microenvironment of chondrocytes, which can promote the secretion of chondrocyte matrix and induce responsive differentiation. Integrin is a heterodimer transmembrane adhesion receptor that provides an important bioactive basis for ECM assembly [66,67]. Integrin, interacts with various intracellular and extracellular ligands and is significant in controlling cell fate [68]. Binding of integrin receptors to cell adhesion ligands of ECM allows integrin receptors to activate cascade signals to connect the cytoskeleton and ECM [14,67]. Cell behavior can be feasibly regulated by adjusting the density of adhesion ligands in nanomaterials [69,70]. In the earlier materials screening of four different LDH nanoparticles, MgAl-Cl and MgFe-NO₃ LDH showed superior effects than other groups, thus were selected for further cell function validation. The ion compositions of four LDH mainly resulted in different physical-chemical properties and biological function. The metal ion release of materials lead to difference in

cellular adhesion, uptake and further signaling pathway influence, thus together form the superior effects of selected LDH than other groups [71]. The present findings show that the active function of ECM and cell adhesion ligands by optimizing LDH, thus leading to the enhanced differentiation and prompting tissue regeneration. In summary, through the design, synthesis, and optimization of LDH nanomaterials, we analyzed the function and mechanism of LDH in promoting IVD regeneration by regulating the differentiation of MSCs.

5. Conclusions

We successfully constructed LDH nanoparticles with different elemental compositions. Our findings reveal that optimized MgFe–NO₃ LDH is highly efficient in promoting the chondrogenesis of hUC-MSCs. The *in vivo* IVD regeneration effects were increased by optimizing LDH-pretreated hUC-MSCs, which showed an excellent repair function. The collective findings reveal the decisive signaling pathway in LDH that promotes differentiation and tissue regeneration by regulating ECM components and focal adhesion signaling pathway. The bioactive and controllable ionic composition design of LDH applied in the regeneration and repair of IDD provides a theoretical basis for clinical transition and further applications.

CRedit authorship contribution statement

Zhaojie Wang: Investigation, Methodology, Data curation, Writing – original draft. **Huiyi Yang:** Investigation, Methodology, Data curation, Writing – original draft. **Xu Xu:** Data curation, Writing – original draft. **Hongxing Hu:** Investigation, animal model construction. **Yuxin Bai:** Methodology, cell culture, nanoparticle synthesis and characterization. **Jian Hai:** Methodology, Project administration. **Liming Cheng:** Conceptualization, Supervision, Project administration. **Rongrong Zhu:** Conceptualization, Supervision, Project administration.

Declaration of competing interest

The authors declare no conflict of interest.

Acknowledgments

This work was financially supported by the INTERNATIONAL COOPERATION Project of National Natural Science Foundation of China (Grant No. 81810001048), the National Natural Science Foundation of China (Grant Nos. 81922039, 81873994, 31727801, 82225027 and 82001308), and Key Basic Research Projects of Shanghai Science and Technology Commission (Grant No. 19JC141470). We thank Editage (www.editage.cn) for the English language editing.

Appendix A. Supplementary data

Supplementary data to this article can be found online at <https://doi.org/10.1016/j.bioactmat.2022.08.023>.

References

- J.P. Urban, S. Roberts, Degeneration of the intervertebral disc [J], *Arthritis Res. Ther.* 5 (3) (2003) 120–130.
- G. Pattappa, Z. Li, M. Peroglio, N. Wismer, M. Alini, S. Grad, Diversity of intervertebral disc cells: phenotype and function [J], *J. Anat.* 221 (6) (2012) 480–496.
- J. Dowdell, M. Erwin, T. Choma, A. Vaccaro, J. Iatridis, S.K. Cho, Intervertebral disk degeneration and repair, *J. Neurosurg.* 80 (3S) (2017) S46–S54.
- M.D. Humzah, R.W. Soames, Human intervertebral disc: structure and function [J], *Anat. Rec.* 220 (4) (1988) 337–356.
- B.G. Ashinsky, E.D. Bonnevie, S.A. Mandalapu, S. Pickup, C. Wang, L. Han, R. L. Mauck, H.E. Smith, S.E. Gullbrand, Intervertebral disc degeneration is associated with aberrant endplate remodeling and reduced small molecule transport [J], *J. Bone Miner. Res.* 35 (8) (2020) 1572–1581.
- T. Vos, A.D. Flaxman, M. Naghavi, R. Lozano, C. Michaud, M. Ezzati, K. Shibuya, J. A. Salomon, S. Abdalla, V. Aboyans, J. Abraham, I. Ackerman, R. Aggarwal, S. Y. Ahn, M.K. Ali, M. Alvarado, H.R. Anderson, L.M. Anderson, K.G. Andrews, C. Atkinson, L.M. Baddour, A.N. Bahalim, S. Barker-Collo, L.H. Barrero, D. H. Bartels, M.G. Basáñez, A. Baxter, M.L. Bell, E.J. Benjamin, D. Bennett, E. Bernabé, K. Bhalla, B. Bhandari, B. Bikbov, A. Bin Abdulhak, G. Birbeck, J. A. Black, H. Blencowe, J.D. Blore, F. Blyth, I. Bolliger, A. Bonaventure, S. Boufous, R. Bourne, M. Boussinesq, T. Braithwaite, C. Brayne, L. Bridgett, S. Brooker, P. Brooks, T.S. Brugha, C. Bryan-Hancock, C. Bucello, R. Buchbinder, G. Buckle, C. M. Budke, M. Burch, P. Burney, R. Burstein, B. Calabria, B. Campbell, C.E. Canter, H. Carabin, J. Carapetis, L. Carmona, C. Cella, F. Charlson, H. Chen, A.T. Cheng, D. Chou, S.S. Chugh, L.E. Coffeng, S.D. Colan, S. Colquhoun, K.E. Colson, J. Condon, M.D. Connor, L.T. Cooper, M. Corriere, M. Cortinovis, K.C. de Vaccaro, W. Couser, B.C. Cowie, M.H. Criqui, M. Cross, K.C. Dabhadkar, M. Dahiya, N. Dahodwala, J. Damsere-Derry, G. Danaei, A. Davis, D. De Leo, L. Degenhardt, R. Dellavalle, A. Delossantos, J. Denenberg, S. Derrett, D.C. Des Jarlais, S. D. Dharmaratne, M. Dherani, C. Diaz-Torne, H. Dolk, E.R. Dorsey, T. Driscoll, H. Duber, B. Ebel, K. Edmond, A. Elbaz, S.E. Ali, H. Erskine, P.J. Erwin, P. Espindola, S.E. Ewoigbokhan, F. Farzadfar, V. Feigin, D.T. Felson, A. Ferrari, C. P. Ferri, E.M. Fèvre, M.M. Finucane, S. Flaxman, L. Flood, K. Foreman, M. H. Forouzanfar, F.G. Fowkes, R. Franklin, M. Fransen, M.K. Freeman, B.J. Gabbe, S. E. Gabriel, E. Gakidou, H.A. Ganatra, B. Garcia, F. Gaspari, R.F. Gillum, G. Gmel, R. Gosselin, R. Grainger, J. Groeger, F. Guillemin, D. Gunnell, R. Gupta, J. Haagsma, H. Hagan, Y.A. Halasa, W. Hall, D. Haring, J.M. Haro, J.E. Harrison, R. Havmoeller, R.J. Hay, H. Higashi, C. Hill, B. Hoen, H. Hoffman, P.J. Hotze, D. Hoy, J.J. Huang, S.E. Ibeanusi, K.H. Jacobsen, S.L. James, D. Jarvis, R. Jasrasaria, S. Jayaraman, N. Johns, J.B. Jonas, G. Karthikeyan, N. Kassebaum, N. Kawakami, A. Keren, J.P. Khoo, C.H. King, L.M. Knowlton, O. Kobusingye, A. Koranteng, R. Krishnamurthi, R. Laloo, L.L. Laslett, T. Lathlean, J.L. Leasher, Y. Y. Lee, J. Leigh, S.S. Lim, E. Limb, J.K. Lin, M. Lipnick, S.E. Lipshultz, W. Liu, M. Loane, S.L. Ohno, R. Lyons, J. Ma, J. Mabweijano, M.F. MacIntyre, R. Malekzadeh, L. Mallinger, S. Manivannan, W. Marcenes, L. March, D.J. Margolis, G.B. Marks, R. Marks, A. Matsumori, R. Matzopoulos, B.M. Mayosi, J.H. McAnulty, M.M. McDermott, N. McGill, J. McGrath, M.E. Medina-Mora, M. Meltzer, G. A. Mensah, T.R. Merriman, A.C. Meyer, V. Miglioli, M. Miller, T.R. Miller, P. B. Mitchell, A.O. Mocumbi, T.E. Moffitt, A.A. Mokdad, L. Monasta, M. Montico, M. Moradi-Lakeh, A. Moran, L. Morawska, R. Mori, M.E. Murdoch, M.K. Mwaniki, K. Naidoo, M.N. Nair, L. Naldi, K.M. Narayan, P.K. Nelson, R.G. Nelson, M. C. Nevitt, C.R. Newton, S. Nolte, P. Norman, R. Norman, M. O'Donnell, S. O'Hanlon, C. Olives, S.B. Omer, K. Ortblad, R. Osborne, D. Ozgediz, A. Page, B. Pahari, J.D. Pandian, A.P. Rivero, S.B. Patten, N. Pearce, R.P. Padilla, F. Perez-Ruiz, N. Perico, K. Pesudovs, D. Phillips, M.R. Phillips, K. Pierce, S. Pion, G. V. Polanczyk, S. Polinder, C.A. Pope 3rd, S. Popova, E. Porrini, F. Pourmalek, M. Prince, R.L. Pullan, K.D. Ramaiah, D. Ranganathan, H. Razavi, M. Regan, J. T. Rehm, D.B. Rein, G. Remuzzi, R. Richardson, F.P. Rivara, T. Roberts, C. Robinson, F.R. De León, L. Ronfani, R. Room, L.C. Rosenfeld, L. Rushton, R. L. Sacco, S. Saha, U. Sampson, L. Sanchez-Riera, E. Sanman, D.C. Schwebel, J. G. Scott, M. Segui-Gomez, S. Shahrzad, D.S. Shepard, H. Shin, R. Shivakoti, D. Singh, G.M. Singh, J.A. Singh, J. Singleton, D.A. Sleet, K. Sliwa, E. Smith, J.L. Smith, N. J. Stapelberg, A. Steer, T. Steiner, W.A. Stolk, L.J. Stovner, C. Sudfeld, S. Syed, G. Tamburlini, M. Tavakkoli, H.R. Taylor, J.A. Taylor, W.J. Taylor, B. Thomas, W. M. Thomson, G.D. Thurston, I.M. Tleyjeh, M. Tonelli, J.A. Towbin, T. Truelsen, M. K. Tsilimbaris, C. Ubeda, E.A. Undurraga, M.J. van der Werf, J. van Os, M. S. Vavilala, N. Venketasubramanian, M. Wang, W. Wang, K. Watt, D.J. Weatherall, M.A. Weinstock, R. Weintraub, M.G. Weisskopf, M.M. Weissman, R.A. White, H. Whiteford, S.T. Wiersma, J.D. Wilkinson, H.C. Williams, S.R. Williams, E. Witt, F. Wolfe, A.D. Woolf, S. Wulf, P.H. Yeh, A.K. Zaidi, Z.J. Zheng, D. Zonies, A. D. Lopez, C.J. Murray, M.A. AlMazrou, Z.A. Memish, Years lived with disability (YLDs) for 1160 sequelae of 289 diseases and injuries 1990–2010: a systematic analysis for the Global Burden of Disease Study 2010 [J], *Lancet (London, England)* 380 (9859) (2012) 2163–2196.
- A. Cieza, K. Causey, K. Kamenov, S.W. Hanson, S. Chatterji, T. Vos, Global estimates of the need for rehabilitation based on the global burden of disease study 2019: a systematic analysis for the global burden of disease study 2019 [J], *Lancet* 396 (10267) (2021) 2006–2017.
- M.A. Capozza, S. Triarico, S. Mastrangelo, G. Attinà, P. Maurizi, A. Ruggiero, Narrative review of intrathecal drug delivery (IDD): indications, devices and potential complications [J], *Ann. Transl. Med.* 9 (2) (2021) 186.
- K.J. Cho, S.I. Suk, S.R. Park, J.H. Kim, S.S. Kim, W.K. Choi, K.Y. Lee, S.R. Lee, Complications in posterior fusion and instrumentation for degenerative lumbar scoliosis, *Spine (Phila Pa 1976)* 32 (20) (2007) 2232–2237.
- S.M. Eisenstein, B. Balain, S. Roberts, Current treatment options for intervertebral, Disc Pathologies [J], *Cartilage* 11 (2) (2020) 143–151.
- G. Li, L. Ma, S. He, R. Luo, B. Wang, W. Zhang, Y. Song, Z. Liao, W. Ke, Q. Xiang, X. Feng, X. Wu, Y. Zhang, K. Wang, C. Yang, WTAP-mediated m(6A) modification of lncRNA NORAD promotes intervertebral disc degeneration [J], *Nat. Commun.* 13 (1) (2022) 1469.
- T. Kamatani, H. Hagizawa, S. Yarimitsu, M. Morioka, S. Koyamatsu, M. Sugimoto, J. Kodama, J. Yamane, H. Ishiguro, S. Shichino, K. Abe, W. Fujibuchi, H. Fujie, T. Kaito, N. Tsumaki, Human iPSC cell-derived cartilaginous tissue spatially and functionally replaces nucleus pulposus [J], *Biomaterials* 284 (2022), 121491.
- A.N. Khan, H.E. Jacobsen, J. Khan, C.G. Filippi, M. Levine, R.A. Lehman Jr., K. D. Riew, L.G. Lenke, N.O. Chahine, Inflammatory biomarkers of low back pain and disc degeneration: a review [J], *Ann. N. Y. Acad. Sci.* 1410 (1) (2017) 68–84.

- [14] A. De Arcangelis, E. Georges-Labouesse, Integrin and ECM functions: roles in vertebrate development [J], *Trends Genet. : TIG (Trends Genet.)* 16 (9) (2000) 389–395.
- [15] H. Liang, R. Luo, G. Li, W. Zhang, Y. Song, C. Yang, The proteolysis of ECM in intervertebral disc degeneration [J], *Int. J. Mol. Sci.* 23 (3) (2022) 1715–1729.
- [16] J. Clouet, M. Fusellier, A. Camus, C. Le Visage, J. Guicheux, Intervertebral disc regeneration: from cell therapy to the development of novel bioinspired endogenous repair strategies [J], *Adv. Drug Deliv. Rev.* 146 (2019) 306–324.
- [17] A.L.A. Binch, J.C. Fitzgerald, E.A. Gowney, F. Barry, Cell-based strategies for IVD repair: clinical progress and translational obstacles [J], *Nat. Rev. Rheumatol.* 17 (3) (2021) 158–175.
- [18] W. Zhang, T. Sun, Y. Li, M. Yang, Y. Zhao, J. Liu, Z. Li, Application of stem cells in the repair of intervertebral disc degeneration [J], *Stem Cell Res. Ther.* 13 (1) (2022) 70.
- [19] S.W. Lane, D.A. Williams, F.M. Watt, Modulating the stem cell niche for tissue regeneration [J], *Nat. Biotechnol.* 32 (8) (2014) 795–803.
- [20] R.S. Mahla, Stem cells applications in regenerative medicine and disease therapeutics [J], 2016, *Int. J. Cell Biol.* (2016), 6940283.
- [21] Q. Li, H. Yu, M. Sun, P. Yang, X. Hu, Y. Ao, J. Cheng, The tissue origin effect of extracellular vesicles on cartilage and bone regeneration [J], *Acta Biomater.* 125 (2021) 253–266.
- [22] X. Li, A. Wu, C. Han, C. Chen, T. Zhou, K. Zhang, X. Yang, Z. Chen, A. Qin, H. Tian, J. Zhao, Bone marrow-derived mesenchymal stem cells in three-dimensional coculture attenuate degeneration of nucleus pulposus cells [J], *Aging* 11 (20) (2019) 9167–9187.
- [23] C. Cao, J. Zou, X. Liu, A. Shapiro, M. Moral, Z. Luo, Q. Shi, J. Liu, H. Yang, N. Ebraheim, Bone marrow mesenchymal stem cells slow intervertebral disc degeneration through the NF- κ B pathway [J], *Spine J. : official journal of the North American Spine Society* 15 (3) (2015) 530–538.
- [24] H. Ishiguro, T. Kaito, S. Yarimitsu, H. Hashimoto, R. Okada, J. Kushioka, R. Chijimatsu, S. Takenaka, T. Makino, Y. Sakai, Y. Moriguchi, S. Otsuru, D.A. Hart, H. Fujie, N. Nakamura, H. Yoshikawa, Intervertebral disc regeneration with an adipose mesenchymal stem cell-derived tissue-engineered construct in a rat nucleotomy model [J], *Acta Biomater.* 87 (2019) 118–129.
- [25] D.C. Ding, Y.H. Chang, W.C. Shyu, S.Z. Lin, Human umbilical cord mesenchymal stem cells: a new era for stem cell therapy, [J], *Cell transplantation* 24 (3) (2015) 339–347.
- [26] K. Hu, T. Yu, S. Tang, X. Xu, Z. Guo, J. Qian, Y. Cheng, Y. Zhao, S. Yan, H. Zhang, M. Wan, C. Du, Y. Feng, Q. Liu, Z. Gu, B. Chen, F. Zhang, N. Gu, Dual anisotropicity comprising 3D printed structures and magnetic nanoparticle assemblies: towards the promotion of mesenchymal stem cell osteogenic differentiation [J], *NPG Asia Mater.* 13 (1) (2021).
- [27] D.H. Kim, J.T. Martin, S.E. Gullbrand, D.M. Elliott, L.J. Smith, H.E. Smith, R. L. Mauck, Fabrication, maturation, and implantation of composite tissue-engineered total discs formed from native and mesenchymal stem cell combinations [J], *Acta Biomater.* 114 (2020) 53–62.
- [28] H. Zhang, S. Yu, X. Zhao, Z. Mao, C. Gao, Stromal cell-derived factor-1 α -encapsulated albumin/heparin nanoparticles for induced stem cell migration and intervertebral disc regeneration in vivo [J], *Acta Biomater.* 72 (2018) 217–227.
- [29] J. Xu, X.Q. E, N.X. Wang, M.N. Wang, H.X. Xie, Y.H. Cao, L.H. Sun, J. Tian, H. J. Chen, J.L. Yan, BMP7 enhances the effect of BMSCs on extracellular matrix remodeling in a rabbit model of intervertebral disc degeneration [J], *FEBS J.* 283 (9) (2016) 1689–1700.
- [30] Z. Wang, Z. Xu, G. Jing, Q. Wang, L. Yang, X. He, L. Lin, J. Niu, L. Yang, K. Li, Z. Liu, Y. Qian, S. Wang, R. Zhu, Layered double hydroxide eliminate embryotoxicity of chemotherapeutic drug through BMP-SMAD signaling pathway [J], *Biomaterials* 230 (2020), 119602.
- [31] R. Zhu, X. Zhu, Y. Zhu, Z. Wang, X. He, Z. Wu, L. Xue, W. Fan, R. Huang, Z. Xu, X. Qi, W. Xu, Y. Yu, Y. Ren, C. Li, Q. Cheng, L. Ling, S. Wang, L. Cheng, Immunomodulatory layered double hydroxide nanoparticles enable neurogenesis by targeting transforming growth factor-beta receptor 2 [J], *ACS Nano* 15 (2) (2021) 2812–2830.
- [32] H. Fu, L. Wang, Q. Bao, D. Ni, P. Hu, J. Shi, Acid Neutralization and Immune Regulation by Calcium-Aluminum-Layered Double Hydroxide for Osteoporosis Reversion [J], *J Am Chem Soc*, 2022, <https://doi.org/10.1021/jacs.1022c00749>.
- [33] L. Yang, X. He, G. Jing, H. Wang, J. Niu, Y. Qian, S. Wang, Layered double hydroxide nanoparticles with osteogenic effects as miRNA carriers to synergistically promote osteogenesis of MSCs [J], *ACS Appl. Mater. Interfaces* 13 (41) (2021) 48386–48402.
- [34] Y. Wang, S. Shen, T. Hu, G.R. Williams, Y. Bian, B. Feng, R. Liang, X. Weng, Layered double hydroxide modified bone cement promoting osseointegration via multiple osteogenic signal pathways [J], *ACS Nano* 15 (6) (2021) 9732–9745.
- [35] X. He, Y. Zhu, L. Yang, Z. Wang, Z. Wang, J. Feng, X. Wen, L. Cheng, R. Zhu, MgFe-LDH nanoparticles: a promising leukemia inhibitory factor replacement for self-renewal and pluripotency maintenance in cultured mouse embryonic stem cells [J], *Adv. Sci.* 8 (9) (2021), 2003535.
- [36] L. Yang, J. Sun, Q. Liu, R. Zhu, Q. Yang, J. Hua, L. Zheng, K. Li, S. Wang, A. Li, Synergistic functional nanocomposites enhance immunotherapy in solid tumors by remodeling the immunoenvironment [J], *Adv. Sci.* 6 (6) (2019), 1802012.
- [37] A.E. Stamate, O.D. Pavel, R. Zavoianu, I. Brezestean, A. Ciorita, R. Birjega, K. Neubauer, A. Koeckritz, I.C. Marcu, Ce-containing MgAl-layered double hydroxide-graphene oxide hybrid materials as multifunctional catalysts for organic transformations, *J. Mater.* 14 (23) (2021) 7457–7478.
- [38] D. Gopal, A.L. Ho, A. Shah, J.H. Chi, Molecular basis of intervertebral disc degeneration [J], *Adv. Exp. Med. Biol.* 760 (2012) 114–133.
- [39] S. Zhang, B. Hu, W. Liu, P. Wang, X. Lv, S. Chen, Z. Shao, The role of structure and function changes of sensory nervous system in intervertebral disc-related low back pain, *Osteoarthritis Cartilage* 29 (1) (2021) 17–27.
- [40] K. Luoma, H. Riihimäki, R. Luukkonen, R. Raininko, E. Viikari-Juntura, A. Lamminen, Low back pain in relation to lumbar disc degeneration, *Spine (Phila Pa 1976)* 25 (4) (2000) 487–492.
- [41] A. Ertaş, T. Gediz, C. Ozdol, I.A. Gurses, M. Onder, M. Uzel, K. Aghayev, Risk of intervertebral disc joint puncture during lumbar puncture [J], *Clin. Neurol. Neurosurg.* 200 (2021), 106107.
- [42] J. Schol, D. Sakai, Cell therapy for intervertebral disc herniation and degenerative disc disease: clinical trials [J], *Int. Orthop.* 43 (4) (2019) 1011–1025.
- [43] R.D. Bowles, L.A. Setton, Biomaterials for intervertebral disc regeneration and repair [J], *Biomaterials* 129 (2017) 54–67.
- [44] B.G. Ashinsky, S.E. Gullbrand, E.D. Bonnevie, C. Wang, D.H. Kim, L. Han, R. L. Mauck, H.E. Smith, Sacrificial fibers improve matrix distribution and micro-mechanical properties in a tissue-engineered intervertebral disc [J], *Acta Biomater.* 111 (2020) 232–241.
- [45] S. Amukarimi, M. Mozafari, Biodegradable magnesium-based biomaterials: an overview of challenges and opportunities, [J], *MedComm* 2 (2) (2021) 123–144.
- [46] X. He, Y. Zhu, L. Yang, Z. Wang, Z. Wang, J. Feng, X. Wen, L. Cheng, R. Zhu, MgFe-LDH nanoparticles: a promising leukemia inhibitory factor replacement for self-renewal and pluripotency maintenance in cultured mouse embryonic stem cells [J], *Adv. Sci.* 8 (9) (2021), 2003535.
- [47] Z. Wang, H. Yang, Y. Bai, L. Cheng, R. Zhu, rBMSC osteogenic differentiation enhanced by graphene quantum dots loaded with immunomodulatory layered double hydroxide nanoparticles [J], *Biomed. Mater.* 17 (2) (2022), 024101.
- [48] E. Jahanmard, J. Keramat, A. Nasirpour, R. Emadi, Efficiency of calcined Aluminum-Magnesium layered double hydroxide for adsorption of aflatoxin M(1) from solution and matrix of milk [J], *J. Food Sci.* 86 (12) (2021) 5200–5212.
- [49] Z. Wang, P. Liang, X. He, B. Wu, Q. Liu, Z. Xu, H. Wu, Z. Liu, Y. Qian, S. Wang, R. Zhu, Etoposide loaded layered double hydroxide nanoparticles reversing chemoresistance and eradicating human glioma stem cells in vitro and in vivo [J], *Nanoscale* 10 (27) (2018) 13106–13121.
- [50] R. Tiruvannamalai Annamalai, D.R. Mertztz, E.L. Daley, J.P. Stegemann, Collagen Type II enhances chondrogenic differentiation in agarose-based modular microtissues, [J], *Cytotherapy* 18 (2) (2016) 263–277.
- [51] Y. Ling, W. Zhang, P. Wang, W. Xie, W. Yang, D.A. Wang, C. Fan, Three-dimensional (3D) hydrogel serves as a platform to identify potential markers of chondrocyte dedifferentiation by combining RNA sequencing [J], *Bioact. Mater.* 6 (9) (2021) 2914–2926.
- [52] S.E. Gullbrand, D.H. Kim, E. Bonnevie, B.G. Ashinsky, L.J. Smith, D.M. Elliott, R. L. Mauck, H.E. Smith, Towards the scale up of tissue engineered intervertebral discs for clinical application [J], *Acta Biomater.* 70 (2018) 154–164.
- [53] M. Fathi-Achachelouei, H. Knopf-Marques, C.E. Ribeiro da Silva, J. Barthes, E. Bat, A. Tezcaner, N.E. Vrana, Use of nanoparticles in tissue engineering and regenerative medicine [J], *Front. Bieng. Biotechnol.* 7 (2019) 113.
- [54] C. Cunha, C.R. Almeida, M.I. Almeida, A.M. Silva, M. Molinos, S. Lamas, C. L. Pereira, G.Q. Teixeira, A.T. Monteiro, S.G. Santos, R.M. Goncalves, M. A. Barbosa, Systemic delivery of bone marrow mesenchymal stem cells for in situ intervertebral disc regeneration [J], *Stem Cells Transl Med* 6 (3) (2017) 1029–1039.
- [55] J. Yang, X. Wang, Y. Fan, X. Song, J. Wu, Z. Fu, T. Li, Y. Huang, Z. Tang, S. Meng, N. Liu, J. Chen, P. Liu, L. Yang, X. Gong, C. Chen, Tropoelastin improves adhesion and migration of intra-articular injected infrapatellar fat pad MSCs and reduces osteoarthritis progression [J], *Bioact. Mater.* 10 (2022) 443–459.
- [56] A. Krouwels, F.P.W. Melchels, M.H.P. van Rijen, C.B.M. Ten Brink, W.J.A. Dhert, F. Cuihur Oner, M.A. Tryfonidou, L.B. Creemers, Focal adhesion signaling affects regeneration by human nucleus pulposus cells in collagen- but not carbohydrate-based hydrogels [J], *Acta Biomater.* 66 (2018) 238–247.
- [57] P. Kanchanawong, G. Shtengel, A.M. Pasapera, E.B. Ramko, M.W. Davidson, H. F. Hess, C.M. Waterman, Nanoscale architecture of integrin-based cell adhesions [J], *Nature* 468 (7323) (2010) 580–584.
- [58] G. Nardone, J. Oliver-De La Cruz, J. Vrbsky, C. Martini, J. Pribyl, P. Skládál, M. Pešl, G. Caluori, S. Pagliari, F. Martino, Z. Maceckova, M. Hajdich, A. Sanz-Garcia, N.M. Pugno, G.B. Stokin, G. Forte, YAP regulates cell mechanics by controlling focal adhesion assembly [J], *Nat. Commun.* 8 (2017), 15321.
- [59] C. Celik, A. Franco-Obregón, E.H. Lee, J.H. Hui, Z. Yang, Directionalities of magnetic fields and topographic scaffolds synergize to enhance MSC chondrogenesis [J], *Acta Biomater.* 119 (2021) 169–183.
- [60] T. Koshimizu, M. Kawai, H. Kondou, K. Tachikawa, N. Sakai, K. Ozono, T. Michigami, Vinculin functions as regulator of chondrogenesis [J], *J. Biol. Chem.* 287 (19) (2012) 15760–15775.
- [61] Y. Jiang, C. Zhang, L. Long, L. Ge, J. Guo, Z. Fan, G. Yu, A comprehensive analysis of SE-lncRNA/mRNA differential expression profiles during chondrogenic differentiation of human bone marrow mesenchymal stem cells [J], *Front. Cell Dev. Biol.* 9 (2021), 721205.
- [62] D. Huang, M. Khoe, M. Befekadu, S. Chung, Y. Takata, D. Ilic, M. Bryer-Ash, Focal adhesion kinase mediates cell survival via NF-kappaB and ERK signaling pathways [J], *Am. J. Physiol. Cell Physiol.* 292 (4) (2007) C1339–C1352.
- [63] P.S. Mathieu, E.G. Lobo, Cytoskeletal and focal adhesion influences on mesenchymal stem cell shape, mechanical properties, and differentiation down osteogenic, adipogenic, and chondrogenic pathways, *J. Tissue Eng. Part B Rev* 18 (6) (2012) 436–444.
- [64] G. Vadala, L. Ambrosio, F. Russo, R. Papalia, V. Denaro, Interaction between mesenchymal stem cells and intervertebral disc microenvironment: from cell therapy to tissue engineering [J], 2019, *Stem Cell. Int.* (2019), 2376172.

- [65] S. de Vries, M.V. Doeselaar, B. Meij, M. Tryfonidou, K. Ito, Notochordal cell matrix as a therapeutic agent for intervertebral disc regeneration [J], *tissue engineering, Part. Accel.* 25 (11–12) (2019) 830–841.
- [66] J. Koivunen, H. Tu, A. Kemppainen, P. Anbazhagan, M.A. Finnilä, S. Saarakkala, J. Käpylä, N. Lu, A. Heikkinen, A.H. Juffer, J. Heino, D. Gullberg, T. Pihlajaniemi, Integrin $\alpha 11\beta 1$ is a receptor for collagen XIII, [J], *Cell and tissue research* 383 (3) (2021) 1135–1153.
- [67] F. Li Mow Chee, A. Byron, Network analysis of integrin adhesion complexes [J], *methods in molecular biology (clifton, N. J.)* 2217 (2021) 149–179.
- [68] J.Z. Kechagia, J. Ivaska, P. Roca-Cusachs, Integrins as biomechanical sensors of the microenvironment [J], *Nature reviews, Molecular cell biology* 20 (8) (2019) 457–473.
- [69] G. Jing, K. Li, F. Sun, J. Niu, R. Zhu, Y. Qian, S. Wang, Layer-number-dependent effects of graphene oxide on the pluripotency of mouse embryonic stem cells through the regulation of the interaction between the extracellular matrix and integrins [J], *Int. J. Nanomed.* 16 (2021) 3819–3832.
- [70] C. Borrelli, C.T. Buckley, Injectable disc-derived ECM hydrogel functionalised with chondroitin sulfate for intervertebral disc regeneration [J], *Acta Biomater.* 117 (2020) 142–155.
- [71] Z. Liao, H. Liu, L. Ma, J. Lei, B. Tong, G. Li, W. Ke, K. Wang, X. Feng, W. Hua, S. Li, C. Yang, Engineering extracellular vesicles restore the impaired cellular uptake and attenuate intervertebral disc degeneration [J], *ACS Nano* 15 (9) (2021) 14709–14724.